NJC

ROYAL SOCIETY OF CHEMISTRY

PAPER

View Article Online
View Journal | View Issue

Cite this: *New J. Chem.*, 2024, **48**, 17650

Visible light: shaping chemical intelligence in proteinoid–ZnO interfaces†

Panagiotis Mougkogiannis, * Noushin Raeisi Kheirabadi and Andrew Adamatzky

Received 28th August 2024,
Accepted 18th September 2024

DOI: 10.1039/d4nj03803g

rsc.li/njc

We study the emergence of chemical intelligence in proteinoid–ZnO nanocomposites through their interaction with visible light. When these novel materials are exposed to light, they display electrical spiking behaviour that is similar to the action potentials of neurons. We examine the influence of various light conditions, such as wavelength, intensity, and duration, on the photo-response of these nanocomposites. The results indicate that higher light intensity and longer duration are associated with increased frequency and amplitude of voltage spikes. Furthermore, blue light is more effective than red light in this regard. This light-dependent behaviour indicates a form of chemical intelligence, in which the material learns and responds to external stimuli. The results of our research emphasise the potential of proteinoid–ZnO nanocomposites to develop bio-inspired, light-sensitive systems, which can lead to advancements in areas such as photocatalysis, unconventional computing, and adaptive materials. This study enhances the understanding of chemical intelligence and how it is demonstrated in synthetic nanomaterials.

1. Introduction

Zinc oxide (ZnO) is a wide band-gap semiconductor with a direct band gap energy of 3.37 eV.[1–4] This implies that it has the ability to capture photons with energy levels exceeding 3.37 eV, resulting in the emission of electrons and holes. ZnO nanoparticles possess the ability to react to visible light, rendering them highly intriguing for various applications such as photocatalysis, sensors, and electronics.[5–7]

The visible light response of ZnO nanoparticles is attributed to the quantum confinement effect.[2,8] The phenomenon arises when the dimensions of a semiconductor nanoparticle are smaller than the Bohr radius of the electron. In this scenario, the electrons' energy levels are quantized, implying their existence is restricted to discrete energy levels. The quantization of energy levels results in a blue shift in the absorption spectrum of nanoparticles, enabling them to absorb photons of lower energy compared to the bulk material. Doping ZnO nanoparticles with other elements can enhance the quantum confinement effect. Doping involves introducing impurities into a semiconductor material to alter its characteristics. Doping ZnO nanoparticles with gallium, indium, or aluminium can result in a greater blue shift in the absorption spectrum and enhanced photocatalytic activity.[9–11]

The photocatalytic activity of ZnO nanoparticles arises from their ability to generate electron–hole pairs upon light exposure. The electron–hole pairs have the ability to interact with water and oxygen, resulting in the formation of reactive oxygen species (ROS), including hydroxyl radicals and superoxide anions.[12,13] Reactive oxygen species (ROS) exhibit high reactivity and have the ability to oxidise a wide range of organic and inorganic compounds.[14–16] ZnO nanoparticles show promise in the degradation of various pollutants, including dyes, pesticides, and bacteria.[17–19]

ZnO nanoparticles exhibit sensitivity to various stimuli, including electric fields, magnetic fields, and temperature, in addition to their photocatalytic activity.[20–25] This renders them viable candidates for various applications, including sensors, actuators, and electronic devices. ZnO colloidal nanoparticles have demonstrated the ability to interact with proteinoids,[26,27] in addition to their potential applications in photocatalysis, sensors, and electronics.

Proteinoids are artificial polypeptides that demonstrate similar characteristics to those of natural proteins. Proteinoids possess the ability to autonomously form complex structures and engage in molecular interactions, including those with DNA.[28,29] Proteinoids are synthesised by subjecting amino acids to thermal polymerization. Microspheres are membrane-enclosed spherical structures that exhibit the ability to self-assemble.[30–33] The unique characteristics of these molecules render them viable options for unconventional computing devices. The microspheres display oscillatory behaviours and can synchronise their reactions during interaction. The observed collective behaviour has the potential to be utilised in biomolecular-based computing applications. The mechanisms underlying the self-organization and complex dynamics of synthetic polypeptides remain incompletely understood.

Unconventional Computing Laboratory, UWE, Bristol, UK.
E-mail: Panagiotis.Mougkogiannis@uwe.ac.uk

† Electronic supplementary information (ESI) available. See DOI: https://doi.org/10.1039/d4nj03803g

Further study has provided strong proof for the polypeptide nature of proteinoids, despite initial reports suggesting non-peptide bonds and amino acid crosslinking. Fox and Harada (1958) showed that proteinoids are created by the thermal polymerisation of amino acids, leading to the formation of structures containing peptide bonds.[34] Rohlfing's (1976) Fourier transform infrared spectroscopy (FTIR) analysis provided confirmation of the existence of peptide bonds in proteinoids. This was demonstrated through the observation of distinct amide I and amide II bands.[35,36] Additional support is provided by the research conducted by Nakashima and Fox (1980). They used high-performance liquid chromatography (HPLC) to examine proteinoid hydrolysates and discovered a composition that closely resembled proteins.[37] In a study conducted by Matsuno (1982), 13C nuclear magnetic resonance (NMR) spectroscopy was utilised to offer further support for the peptide nature of proteinoid bonds.[38] In a recent study, Guttenberg *et al.* (2017) used advanced analytical methods, such as mass spectrometry, to validate the high frequency of peptide bonds in proteinoids. They also acknowledged the existence of certain non-peptide linkages.[39]

One potential avenue for further exploration of proteinoid systems involves their integration with nanoscale inorganic materials. Semiconductor nanoparticles possess optical and electronic capabilities that can interact with the dynamic characteristics of proteinoids. Proteinoid-nanoparticle hybrid systems have recently been created, demonstrating emergent irradiative behaviours when exposed to external stimuli.[26] This suggests that they could be useful in unconventional computing paradigms that rely on interactions between light and matter.

The purpose of this study is to investigate the photo-response of proteinoids–ZnO nanoparticle colloids when they are exposed to visible light irradiation. Studying the photo-activated processes in composite systems like these can provide valuable insights into how complex behaviours emerge from the interaction between proteinoids and semiconductor nanocrystals. Fig. 1 shows a schematic diagram of proteinoids–ZnO colloidal nanoparticles and their photo-response under visible light irradiation. The purpose of investigating proteinoids–ZnO colloidal nanoparticles under visible light irradiation is to discover fundamental principles that can be used to customise their irradiative characteristics. The results could aid in the advancement of proteinoids-inorganic hybrid materials for unconventional computing devices[40,41] that utilise complex photo-responses.

This work investigates the integration of artificial and hybrid chemical intelligence by examining proteinoid–ZnO nanocomposites. Chemical intelligence spans a wide range of systems, including both naturally occurring biological networks and artificially designed ones, as shown in Fig. 2 and Table 1. We are primarily concerned with developing bio-inspired systems that connect artificial and hybrid chemical intelligence. Our objective is to study the light-responsive properties of proteinoid–ZnO nanocomposites to show how these materials display significant features of chemical intelligence. Specifically, they can process information by responding to light stimuli, adapt through modulating their electrical spiking patterns, and exhibit complex behaviours through adjustable photo-responses. This study not only adds to the expanding domain of molecular computers and chemical robots[42] but also takes inspiration from biological neural networks and cellular signalling pathways.[43] Our goal is to use the distinct characteristics of proteinoid–ZnO interfaces to enhance our knowledge of chemical intelligence and provide new possibilities in adaptive materials, bio-inspired computers, and synthetic biology.[44,45] This study aims to showcase the ability to use visible light to manipulate and regulate chemical behaviour in synthetic nanomaterials, hence creating opportunities for the advancement of intelligent and adaptable systems.

2. Methods

Mixing proteinoids with ZnO nanoparticles in water and dimethyl sulfoxide (DMSO) was needed to make bio-hybrid composite materials, as shown in Fig. 3. Poly-glutamic acid:-arginine protein-like chains were synthesised by thermally polymerizing L-glutamic acid and L-arginine in a round-bottom flask with a volume of approximately 100 ml. The reaction took place under reflux conditions at a temperature of 180 °C. The process of lyophilization resulted in the formation of a solid proteinoid powder, which was subsequently re-suspended to achieve a concentration of 10 mg mL^{-1}.

To create a homogenous surfactant solution, sodium dodecyl sulfate (SDS) was added to deionized water (DIW) at a concentration of 0.22 wt% and agitated. 1 mg ZnO nanoparticles were introduced to dimethyl sulfoxide (DMSO) while continuously stirring. The concentration of the resultant dispersion was kept at 0.11 mg mL^{-1}. The final suspension was immersed in an ultrasonic bath for 30 minutes. The stirring operation was then repeated for a few hours to achieve a homogeneous dispersion of ZnO.[4] The proteinoid and ZnO

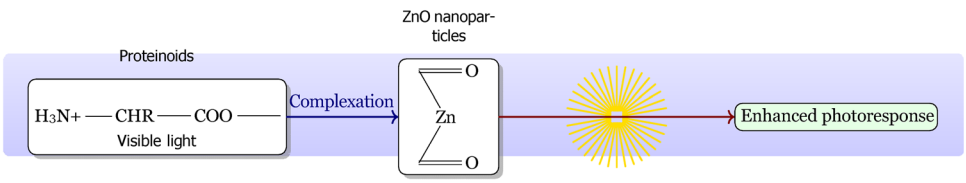

Fig. 1 Conceptual illustration of proteinoids–ZnO colloidal nanoparticles and their photo-response to visible light. Proteinoids, synthetic amino acid polymers forming microspheres, combine with ZnO nanoparticles (zinc oxide nanocrystals with a wide band gap). This combination produces electrical spiking activity resembling neuronal action potentials. Visible light exposure modulates this activity, enhancing reactive oxygen species (ROS) production and the overall photo-response of the complex.

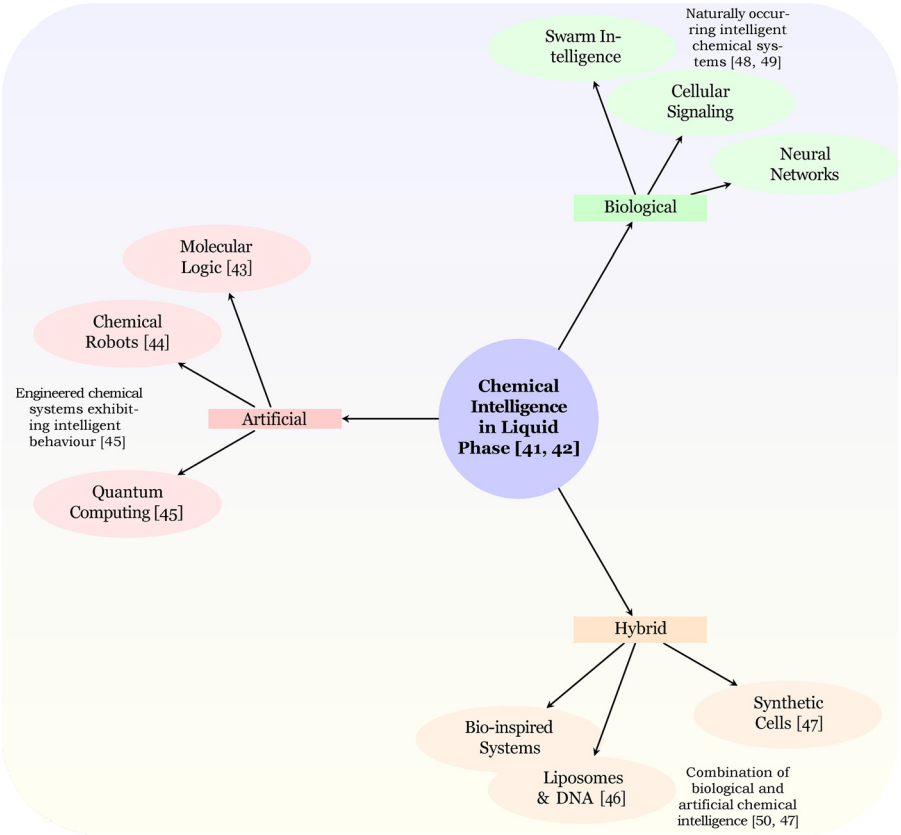

Fig. 2 An overview of the various forms of chemical intelligence and their interconnections. The diagram provides a definition of chemical intelligence, referring to intelligent chemical systems in the liquid phase.[46] It also illustrates the three main classifications: biological, artificial, and hybrid. Biological chemical intelligence involves the study of natural systems that deal with chemical information. Examples of these systems include neural networks, cellular signalling, and swarm intelligence displayed by multicellular organisms.[43,47] Artificial chemical intelligence involves the development of engineered systems that replicate intelligent behaviour through chemical processes.[48] These examples include molecular logic for processing Boolean and fuzzy logic,[49,50] chemical robots, and quantum computing implemented *via* chemical systems.[48] Hybrid chemical intelligence combines elements from biological and artificial systems.[44] Some examples in this field of study involve bio-inspired systems, the use of liposomes and DNA for information processing,[51] and the advancement of synthetic cells with life-like characteristics.[52] The arrows demonstrate the direction and interconnection of these concepts, emphasising the capacity of chemical systems to adapt, process information, and exhibit complex behaviour similar to biological or artificial intelligence.

components were blended in predetermined proportions and physically agitated to attain homogeneous dispersions.[26]

The use of a simple and direct method led to the successful formation of colloidal suspensions containing ZnO nanoparticles enveloped by proteinoids (Fig. 4). Blending enabled the proteinoid shell and inorganic core to interact through electrostatic and hydrophobic forces, eliminating the need for chemical crosslinking or complex conjugation methods. By employing the flexible blend approach, we were able to intentionally manipulate the proteinoid content. This allowed us to study the impact of composition on the photo-physical response. The structure of the proteinoids were analysed using FEI Quanta 650 equipment for scanning electron microscopy (SEM).

The protenoid-inorganic composites were exposed to visible light using a Photonics F3000 system. This system was equipped with LED light sources from World Precision Instruments. The samples were exposed to different spectra, including yellow (590 nm, Part No: 593-30-003), red (625 nm, Part No: 59330004), blue (470 nm, Part No: 59330001), green (525 nm, Part No: 59330002), grey (50%, Part No: 59330221), and broadband daylight (Part No: 59330005). The LEDs emit light with narrowband spectra, which have bandwidths ranging from 25 to 35 nm. The light intensity was adjusted between 20% and 100% of the maximum power density, which was set at 30 mW for the unfiltered daylight LED.

We used a high-resolution data logger with a 24-bit A/D converter (ADC-24, Pico Technology, UK) to measure the proteinoids' electrical activity. We inserted iridium-coated stainless steel sub-dermal needle electrodes (Spes Medica S.r.l., Italy) into the proteinoids and left about 10 mm of space between each electrode pair. This allowed us to measure the difference in electrical potential between them. We recorded one sample per second of all the electrical activity. The data recorder also took several readings (up to 600 per second) and averaged them for further analysis. The timescales for light exposure varied from seconds to hours. The LED system, which can be customised, allowed for a systematic investigation of the dependence of the protenoid–ZnO photo-response on various

Table 1 Overview of chemical intelligence systems. The table presents a selection of notable chemical systems that exhibit complex behaviours and information processing capabilities. The Belousov–Zhabotinsky (BZ) reaction is a prime example of an oscillating chemical reaction that displays complex spatiotemporal patterns and self-organization. The Oregonator model provides a mathematical framework for understanding the dynamics of the BZ reaction. Chemical turing patterns demonstrate the emergence of stationary patterns through reaction–diffusion processes, while the Briggs–Rauscher reaction showcases another oscillating chemical system with periodic colour changes. Reaction–diffusion computers leverage the properties of chemical reactions and diffusion to perform computations, offering a novel approach to unconventional computing. Additionally, the Orban reaction, CIMA–CDIMA reaction, and pH oscillators are included as notable examples of oscillatory chemical systems used as neural surrogates[53]

Chemical system	Description	Ref.
Belousov–Zhabotinsky (BZ) reaction	Oscillating chemical reaction exhibiting complex spatiotemporal patterns and self-organization.	54 and 55
Oregonator model	Simplified mathematical model of the BZ reaction capturing its essential dynamics.	55
Chemical turing patterns	Stationary chemical patterns formed by reaction–diffusion systems, demonstrating symmetry breaking and self-organization.	56 and 57
Briggs–Rauscher reaction	Another oscillating chemical reaction showing periodic colour changes and complex dynamics.	58
Reaction–diffusion computers	Unconventional computing paradigm using chemical reactions and diffusion to perform computations.	44 and 59
Orban reaction	Oscillatory chemical system based on the iodate-sulfite-thiosulfate reaction, used as a neural surrogate.	60
CIMA–CDIMA reaction	Chlorite–iodide–malonic acid (CIMA) and chlorine dioxide–iodine–malonic acid (CDIMA) oscillatory reactions, exhibiting complex dynamics and used as neural surrogates.	61 and 62
pH oscillators	Chemical oscillators based on pH changes, such as the bromite–sulfite and hydrogen peroxide–sulfite–ferrocyanide reactions, used as neural surrogates.	63 and 64

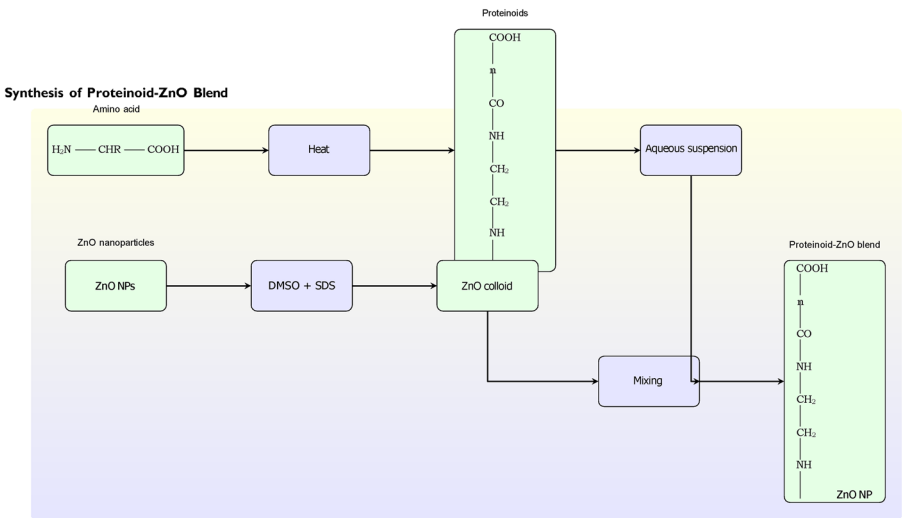

Fig. 3 Schematic illustration of the proteinoid–ZnO blend manufacturing process. Proteinoids are synthesized through thermal polymerization of amino acids and suspended in aqueous solutions. Zinc oxide (ZnO) nanoparticles are synthesized using the sol–gel method with sodium dodecyl sulfate (SDS) surfactant. The proteinoids and ZnO nanoparticles are then combined to create the integrated bio-nano composite material.

factors such as wavelength, intensity, and exposure duration. In order to measure the intensity of light exposure, calibration measurements were conducted using a Light Metre (PRO ILM 1337), as depicted in Fig. S24 (ESI†). The illuminance in lux at the sample stage was measured at different light intensity percentage settings, ranging from 25% to 100%. A nonlinear relationship was observed, indicating saturation at higher intensities.

The calibration data was best fitted by a cubic polynomial, as indicated by the *R*-squared values. The calibration curve allows for the conversion of programmed relative intensity percentages to actual sample illu–minance. The calibrated intensities were used in the proteinoid irradiation experiments to ensure controlled light exposure throughout the visible range.

Fitting of the calibration data found a cubic polynomial model provided the best fit with an R^2 of 0.999.

The resulting calibration equations enable conversion between intensity percentage and illuminance:

$$\text{Linear: } y = 2.43x - 66.04$$

$$\text{Quadratic: } y = 0.01x^2 + 1.66x - 46.89$$

$$\text{Cubic: } y = -0.00x^3 + 0.31x^2 - 15.57x + 226.76$$

For example, the models predict an illuminance of 27.44 lux at 20% intensity. These calibrated conversions allowed controlled visible light exposure of proteinoid–inorganic samples across a range of well-defined intensities.

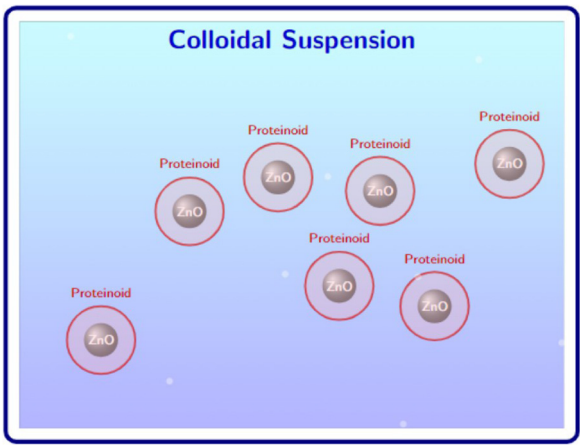

Fig. 4 Schematic representation of ZnO nanoparticles encapsulated by proteinoid materials in a colloidal suspension. The gray spheres represent ZnO nanoparticles, while the red circles depict proteinoid materials. The cyan-blue gradient background represents the colloidal suspension. This illustration demonstrates the simple yet effective method for creating colloidal suspensions of ZnO nanoparticles surrounded by protein-based materials.

3. Results

3.1. Morphological analysis of proteinoid assemblies by scanning electron microscopy

High-resolution SEM imaging revealed that the protenoids produced by thermal polymerization self-assembled into distinct nanostructured morphologies. The scanning electron microscopy (SEM) images in Fig. 5 depict proteinoid microspheres, ZnO nanoparticles, and proteinoid–ZnO nanoparticle composites. Fig. 5a shows the proteinoid microspheres, which have a spherical shape and sizes ranging from 1–5 μm. These microspheres bear a resemblance to primitive protocells. It is worth mentioning that certain proteinoid microspheres exhibit budding-like structures. This observation suggests a possible mechanism for the reproduction and growth of protocells. The morphology of ZnO nanoparticles in Fig. 5b exhibits a smaller size distribution in comparison to the proteinoid microspheres. The individual nanoparticles have measurements of approximately 50–100 nm. The proteinoid–ZnO nanoparticle composites, depicted in Fig. 5c, exhibit the effective integration of ZnO nanoparticles into the proteinoid matrix, resulting in the formation of hybrid structures. Embedding ZnO nanoparticles into proteinoid microspheres can enhance their structural stability and introduce new functionalities, such as improved photoresponse and catalytic activity. The combination of proteinoids and inorganic nanoparticles, as shown by the SEM images, offers a potential method for developing complex and functional protocell models. This helps to connect prebiotic chemistry with the formation of early life-like systems. Clarification of hierarchical self-assembly processes will reveal connections between proteinoid morphology and emergent functions. The ability to structurally organise at the nanoscale with defined order is analogous to protein folding and could enable the engineering of protenoid scaffolds for unconventional computing devices.[65–67]

3.2. Photo-responses under visible light irradiation

The effects of proteinoid composition on the photo-responses of L-Glu : L-Arg–ZnO colloidal nanoparticles were investigated by characterising them under visible light irradiation. The composite exhibited sensitivity and photo-current generation dependent on the proteinoid ratio, as demonstrated in Fig. 6. The transient electrical potential profiles clearly illustrate this relationship. It is worth mentioning that the proteinoid nanoparticles with a ratio of 60–40% exhibited significantly improved photo-responses and photo-electrochemical activity when compared to nanoparticles with lower or higher ratios. This indicates the importance of achieving an optimal balance of interfacial interactions between the proteinoids and ZnO nanocrystals.

The cooperative coupling between the components extends across the visible range, as indicated by the broad spectral

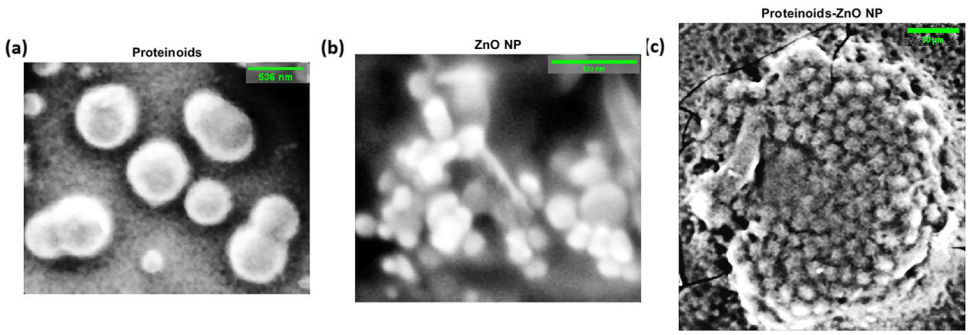

Fig. 5 Scanning electron microscopy (SEM) images of (a) proteinoid microspheres, (b) zinc oxide nanoparticles, and (c) proteinoid–zinc oxide nanoparticle composites. The proteinoid microspheres display a spherical form with dimensions between 1–5 μm, analogous to primordial protocells. Certain proteinoid microspheres exhibit budding-like structures, indicating a possible method for protocell growth and reproduction. The ZnO nanoparticles have a narrower size distribution, with individual nanoparticles ranging from 50 to 100 nm in diameter. In the proteinoid–ZnO nanoparticle composites, ZnO nanoparticles are incorporated into the proteinoid matrix, yielding hybrid structures. The integration of ZnO nanoparticles into proteinoid microspheres could improve their structural stability and offer new capabilities, including increased photoresponse and catalytic activity. The co-assembly of proteinoids and inorganic nanoparticles offers a viable method for developing more complex and functional protocell models, connecting prebiotic chemistry with the origins of early life-like systems.

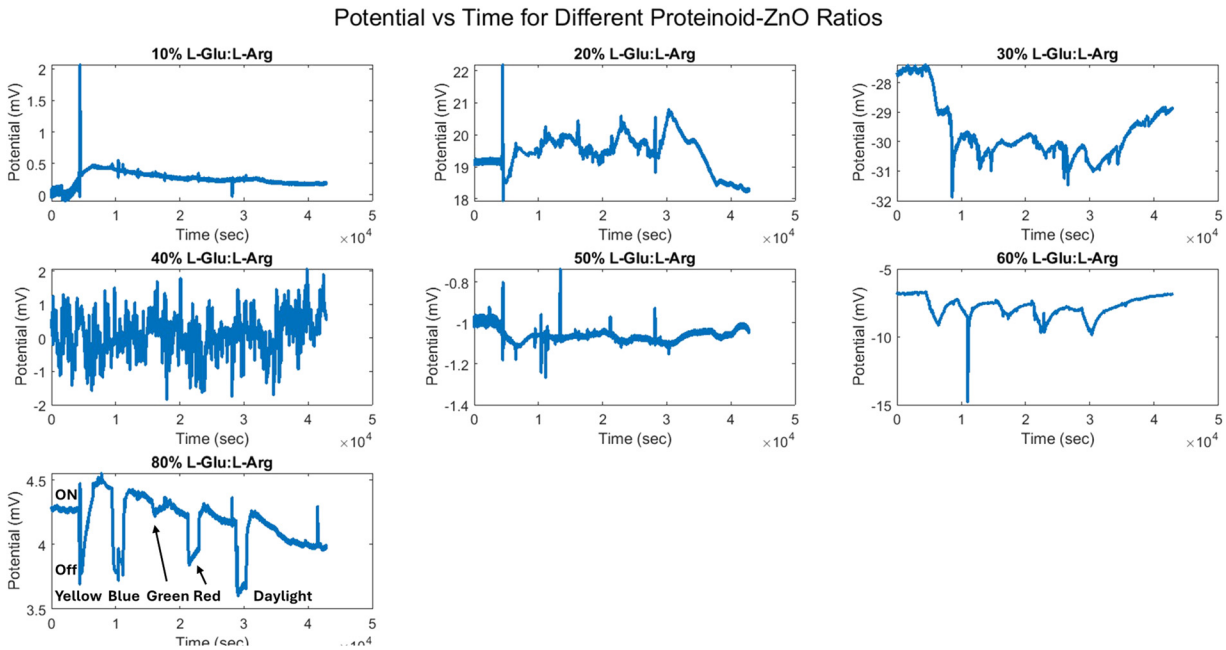

Fig. 6 Photoresponse of L-Glu : L-Arg proteinoid–ZnO nanoparticle composites under visible light irradiation. The photoresponse of colloidal nanoparticles composed of L-Glu, L-Arg, and ZnO was studied under visible light irradiation, with varying proteinoid compositions. The plots display the transient electrical potential profiles for different L-Glu : L-Arg ratios (10%, 20%, 30%, 40%, 50%, 60%, and 80%) when exposed to yellow (λ = 580 nm), blue (λ = 450 nm), green (λ = 532 nm), red (λ = 660 nm), and daylight (broad spectrum) coloured lights. The exposure follows an alternating 30-minute on/off cycle. An increase in proteinoid content leads to higher photoresponses and photoactivity. The highest generation of photocurrent is observed for composite ratios ranging from 40–60%. The enhanced photoresponses across the visible range are supported by the cooperative interfacial effects between the proteinoids and ZnO, as indicated by their broad spectral sensitivity.

sensitivity from yellow to red wavelengths. The proteinoid–inorganic composites exhibit important features of computational functionality, such as spectral sensitivity, adjustable photo-conductivity, and emergent collective responses. These characteristics closely resemble certain aspects of neural systems. The results indicate that these bio-abio hybrids show promise as nanoscale building blocks for unconventional, brain-inspired computing. Current efforts are dedicated to assembling photo-responsive colloids into integrated architectures for all-optical information processing and adaptive"proteinoid brains".

The photo-response of 60 : 40% L-Glu : L-Arg : ZnO nanoparticles under intermittent irradiation with different visible light colours was characterised. As depicted in Fig. 7, six oscillatory peaks were observed following exposure to successive yellow, blue, green, grey, red, and daylight illuminations. The average oscillation period was 4700 ± 100 s, and the standard deviation between peak potentials was 2.0 mV.

Visible spectrum broad spectral sensitivity suggests cooperative interfacial effects between the proteinoid and ZnO components. The peak-to-peak amplitude of 7.6 ± 3.8 mV indicates that the photo-conductance is significantly modulated. On the transient profiles, the median potential is 8.5 ± 0.9 mV, the RMS potential is 7.2 ± 0.7 mV, and the skewness and kurtosis for the oscillation periods are 0.6 and 1.7, respectively.

The distinct photo-response signatures for each colour of light indicate that proteinoid–ZnO colloids have the potential for optical coding. Current research focuses on developing these peptide-nanocrystal composite networks for unconventional computation and neural-like information processing.

Fig. 8 shows the transient photocurrent response of 80 : 20% L-Glu : L-Arg : ZnO nanoparticles under intermittent visible light irradiation. The sample was exposed to 30-minute intervals of yellow, blue, green, red, and white daylight illumination, followed by 30-minute intervals of darkness. In contrast to the 60 : 40% sample, a saturation effect is observed. The restoration of baseline current following each illumination interval exhibits rapid relaxation dynamics.

The photo-response characteristics of L-Glu : L-Arg : ZnO 60 : 40% v/v (P60ZnO) and L-Glu : L-Arg : ZnO 80 : 20% v/v (P80ZnO) nanocomposites were assessed when exposed to visible light. Table 2 provides a summary of the key metrics related to the transient electrical potential profiles. All measurements were conducted under daylight illumination. The daylight source used in this study has a broad spectrum with peak emission around 555 nm, as shown in Fig. S25 (ESI†).

The average oscillation period for the P60ZnO mixture was 4700 ± 100 seconds. The long periodicity suggests a slow intrinsic cycling between the excited and ground state manifolds. The peak-to-peak amplitudes, which were averaged at 7.6 ± 3.8 mV, indicate a significant photomodulation of conductivity. The average root mean square (RMS) potential was 7.2 ± 0.7 mV, and the median value was 8.5 mV. The skewness and kurtosis values for the oscillation periods were 0.6 and 1.7, respectively.

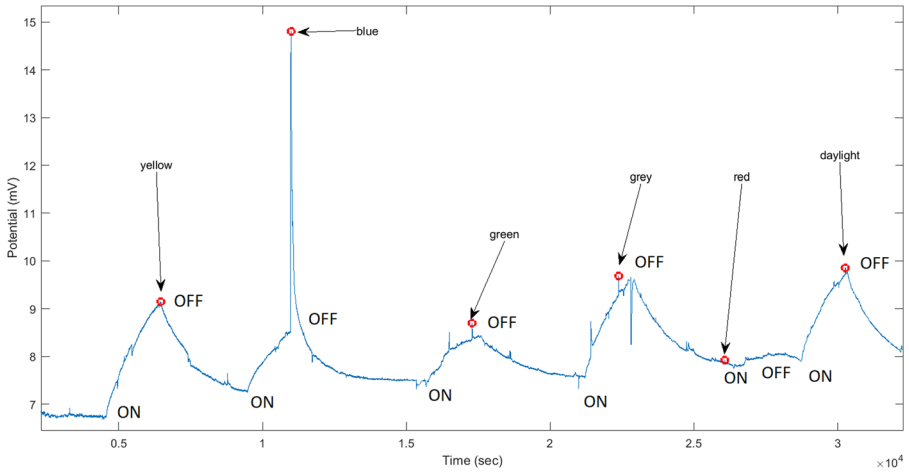

Fig. 7 The figure displays the photo-current response of a sample with a composition ratio of 60 : 40%. The colloidal nanoparticles composed of L-Glu, L-Arg, and ZnO were subjected to intermittent exposure to visible light. The specimen underwent sequential irradiation for a duration of 30 minutes using lights of varying colours, including yellow, blue, green, red, and daylight. For each colour, the light was turned on for 30 minutes and then turned off for 30 minutes. The electrical potential profile exhibits consistent photo-activation and fast signal restoration in the absence of light, indicating the reversible modification of conduction by light. The presence of a wide range of spectral sensitivity within the visible spectrum suggests that there are cooperative interfacial effects occurring between the proteinoid and ZnO components. The evident photoresponse seen in these bio-inorganic composites indicates that they possess promising capabilities as optical sensors and optoelectronic interfaces for adaptive bioelectronic systems.

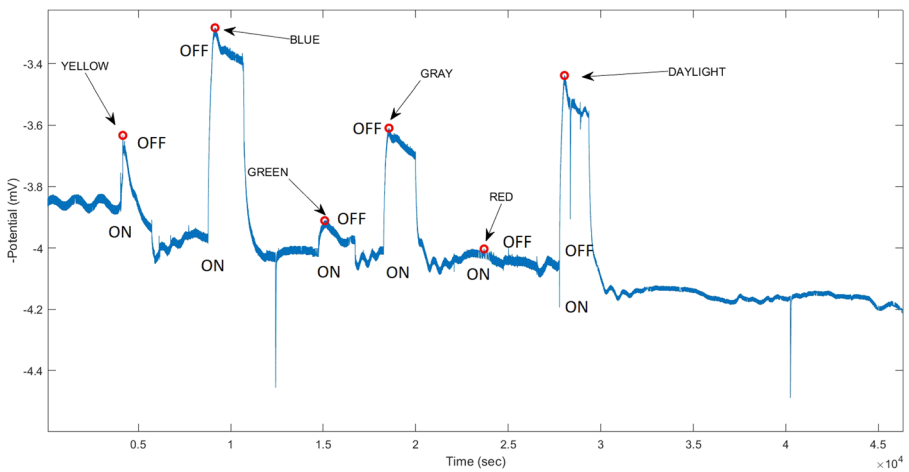

Fig. 8 The transient photocurrent response of 80 : 20% L-Glu : L-Arg : ZnO nanoparticles irradiated intermittently with visible light. The sample was exposed to 30 minute intervals of yellow, blue, green, red, and white daylight illumination followed by 30 minute intervals of darkness. In contrast to the 60 : 40% sample, there is a saturation effect. The restoration of baseline current following each interval of illumination exhibits rapid relaxation dynamics.

On the other hand, the P80ZnO composite exhibited faster oscillations with a shorter period of 2600 ± 600 seconds. However, we observed a decrease in photo-conductivity, as indicated by lower peak-to-peak and RMS amplitudes of 1.0 ± 0.2 mV and 1.5 ± 4.6 mV, respectively. The median potential measured was 4.1 mV. The period skewness and kurtosis values were −0.3 and 1.7, respectively.

The photophysical characteristics of a formulation containing 40% L-Glu, 40% L-Arg, and 60% ZnO were examined when exposed to visible light. According to the data presented in Table 2, this composition displayed periods of instantaneous oscillation. The average peak potential was measured to be 1.7 ± 0.3 mV, while the root mean square (RMS) amplitude was found to be 1.0 ± 0.4 mV. A significant photomodulation between high and low conduction states is indicated by a peak-to-peak magnitude of 2.9 ± 1.0 mV. The analysis of the periodic patterns revealed a distribution that was close to normal, with a skewness value of 0.5 and a kurtosis value of 0.4. In comparison to previous samples, the mixture consisting of 40% proteinoid and 40% colloidal ZnO nanoparticles exhibited faster intrinsic cycling and higher photo-response amplitudes. The data presented in this study demonstrates the effects of proteinoid ratio on photo-physical response mechanisms. Reducing the ZnO content led to faster intrinsic cycling but resulted in smaller magnitudes of photo-response.

The photo-physical characteristics of ZnO colloidal nanoparticles containing a 50 : 50% mixture of L-Glu and L-Arg with

Table 2 Photoresponse characteristics of Px%ZnO nanocomposites from triplicate measurements under different light sources. The light sources used were yellow (λ = 580 nm), blue (λ = 450 nm), green (λ = 532 nm), red (λ = 660 nm), and daylight (broad spectrum). The oscillation period, photoresponse, peak-to-peak voltage, and RMS voltage are reported for each composition. The photoresponse is classified as low, moderate, or high based on the observed electrical potential profiles

Composition	Osc. Period (s)	Photoresponse	Peak to peak (mV)	RMS (mV)
P10%ZnO	—	Low	1.1 ± 1.0	0.20 ± 0.08
P20%ZnO	5300 ± 500	Moderate	4.5 ± 0.6	18.6 ± 0.8
P30%ZnO	4600 ± 200	Moderate	3.1 ± 1.3	29.8 ± 0.7
P40%ZnO	—	Low	2.9 ± 1.0	1.0 ± 0.4
P50%ZnO	5800 ± 900	Moderate	1.4 ± 0.8	1.3 ± 1.0
P60%ZnO	4700 ± 100	High	7.6 ± 3.8	7.2 ± 0.7
P80%ZnO	2600 ± 600	Moderate	1.0 ± 0.2	1.5 ± 4.6

ZnO were evaluated. This evaluation was conducted by taking triplicate measurements while exposing the nanoparticles to visible light. According to the data presented in Fig. 9, the average oscillation period for the three trials was 5800 ± 1400 seconds. The average peak potential was −0.9 ± 1.5 mV, and the average RMS amplitude was 1.3 ± 1.0 mV. A peak-to-peak amplitude of 1.4 ± 0.8 mV suggests that there is a significant photomodulation of conductance occurring, which affects both low and high current states. The median potential remained consistent at −1.1 ± 1.0 mV. The analysis of the oscillation patterns revealed a normal distribution with a mean skewness of 0.5 and a kurtosis of 2.1.

The fact that the photo-response characteristics remain consistent across replicates emphasises the reliability and potential usefulness of these proteinoid–inorganic composite systems.

The photophysical properties of a composite containing 10% L-Glu, 10% L-Arg, and ZnO were analysed and compared to previous studies conducted on formulations with a 50% L-Glu and 50% L-Arg composition. According to the data presented in Table 2, the mixture containing 10% of the proteinoid displayed significantly lower photo-response amplitudes. The average root mean square (RMS) potential was measured to be 0.20 ± 0.08 mV, while the peak-to-peak magnitude was found to be 1.1 ± 1.0 mV, indicating a relatively small range of variation. This indicates that there is minimal photoconductance modulation when compared to the 50 : 50% sample. The 50 : 50% sample showed RMS and peak-to-peak values of 1.3 ± 1.0 mV and 1.4 ± 0.8 mV, respectively.

However, the formulation with a concentration of 10 : 10% L-Glu : L-Arg exhibited a faster intrinsic cycling rate when exposed to light, resulting in shorter oscillation periods. This finding warrants additional evaluation. The reduced photomodulation at this composition suggests that there is less hybridization and interfacial coupling between the proteinoid and inorganic components.

3.3. Relaxation kinetics post-illumination

There is a ''memory'' effect in the proteinoid–ZnO colloids, as evidenced by the continued electrical potential oscillations following exposure to visible light. The proteinoid ratio in the nanocomposites affects the relaxation dynamics and intrinsic cycling, as illustrated in Fig. 10. Notably, post-illumination oscillations with the highest amplitudes were seen in samples with proteinoid contents of 60% and 80%. This increased electrical activity indicates that these composites have the best recall for previous radiation exposure.

The significant ''remembering'' of spectrum stimuli following illumination suggests that these materials may facilitate associative learning and emergent memory in proteinoid-based

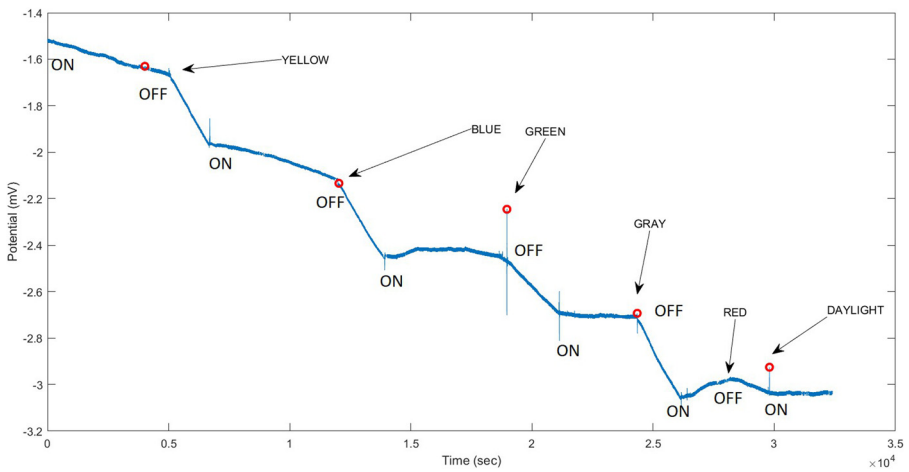

Fig. 9 The photocurrent response of colloidal nanoparticles containing a mixture of 50% L-Glu, 50% L-Arg, and ZnO was studied under visible light irradiation. For each colour, the light was turned on for 30 minutes and then turned off for 30 minutes. The transient electrical potential profile exhibits five oscillation peaks, with an average period of 6400 ± 800 seconds. The peak potentials were averaged to be −2.3 ± 0.5 mV, and they exhibited a peak-to-peak amplitude of 1.6 mV. This suggests that there was significant photo-modulation. The root mean square (RMS) potential measured 2.4 mV, while the median potential was −2.3 mV. The metrics of skewness and kurtosis provide additional characterization of the distributions of oscillation periodicity and amplitude. The unique photo-response signature observed in the 50 : 50% composition indicates that the proteinoid–inorganic interactions have been finely adjusted to enhance photoconductive properties.

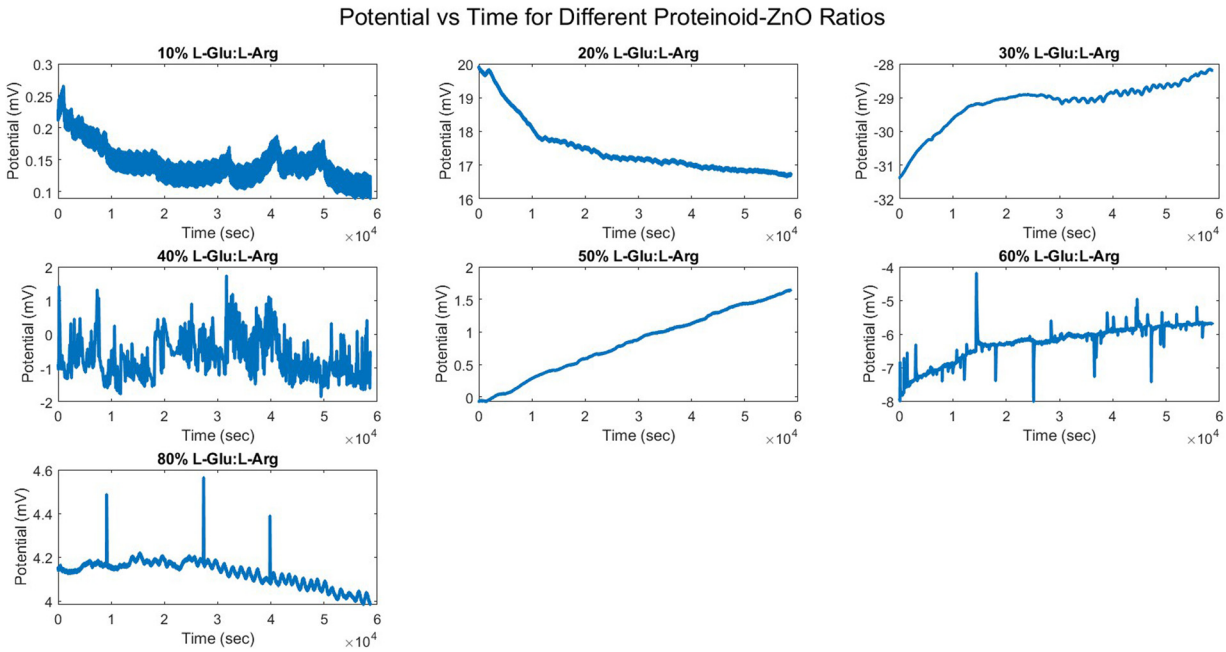

Fig. 10 Post-illumination electrical potential oscillations for L-Glu : L-Arg : ZnO nanoparticles containing between 10% and 80% proteinoid. The samples were initially subjected to intermittent exposure to white, yellow, blue, green, and grey light. Over time, intrinsic oscillatory patterns persisted in the electrical potential after the light was turned off. This "memory" effect demonstrates that visible light modulates the photo-excitation and relaxation dynamics of proteinoid–ZnO. The oscillation kinetics and amplitudes are proportional to the proteinoid ratio, indicating composition-dependent photo-responses.

computing networks. The proteinoid–inorganic photoresponse can be modulated by varying the intensity of daylight, as shown in Fig. 15. Various bio-nano composites consisting of L-Glu : L-Arg : ZnO were exposed to different levels of visible daylight intensity, ranging from low (25%) to medium (50%) and high (100%). The proteinoid ratios in these composites varied from 10% to 80%. The electrical potential profiles exhibit intensity-dependent effects on photo-current generation, oscillation kinetics, and the emergence of spiking behaviours. Reduced light power densities result in a delay in emergence and a decrease in the amplitude of the photo-response. The findings of this study indicate that the modulation of proteinoid–inorganic interactions can be achieved through the manipulation of input light intensity. This aspect will be the primary focus of forthcoming research attempts aimed at developing adaptive technologies.

The colloidal nanoparticles composed of 60% L-Glu : L-Arg, and 40% ZnO demonstrated notable electrical excitability and spiking behaviours that continued even after the cessation of visible light exposure. The presence of oscillatory potentials was found for prolonged durations following irradiation, as depicted in Fig. 11A. The examination of spike timing statistics yielded a mean interval of 2400 ± 600 seconds between spikes, as depicted in Fig. 11B. The amplitudes of the spikes were seen to have an average value of −5.9 ± 0.6 mV, as depicted in Fig. 11C. The Fourier analysis revealed the presence of a prominent low frequency component at 0.042 Hz, which corresponds to the average spike interval (Fig. 11D). This observation showcases the composite material's capacity to retain previous photo-stimulation by means of persistent oscillatory excitation states that resemble brain action potentials. The observed spiking activity of these proteinoid–inorganic hybrids demonstrates their potential as attractive materials for simulating neural dynamics. There exists the possibility of incorporating the photo-response characteristics inspired by the human brain into unconventional computing systems through the manipulation of composition, spectrum sensitivity, and relaxation kinetics.

Both the samples with a ratio of 60 : 40% and 80 : 20% displayed electrical potential spikes, which indicated the presence of persistent excitation states and "photomemory" even after visible light irradiation was stopped. However, several significant differences were observed between the compositions (Fig. 12).

- The 60 : 40% mixture spiked more frequently with a shortened mean interval of 2400 ± 600 s compared to the 80 : 20% sample's 2300 ± 500 s.
- The 60 : 40% formulation had smaller spike amplitude potentials averaging −5.9 ± 0.6 mV *versus* 4.2 ± 0.1 mV for the 80 : 20% composite.
- The dominating spike frequency, as determined by Fourier analysis, was 0.04 Hz for both mixtures.
- The spike amplitudes of the 80 : 20% sample exhibited greater skewness of 1.7 and kurtosis of 5.8 compared to 0.5 and 3.4 for the 60 : 40.

In summary, both compositions demonstrated neural-like spiking behaviours after being illuminated. How-ever, the 80 : 20% sample exhibited larger amplitude spikes that occurred less frequently. Additionally, the spike distribution of the 80 : 20% sample was more skewed and non-normal. This illustrates the ability to adjust the emergent oscillatory dynamics by optimising the proteinoid content. Current

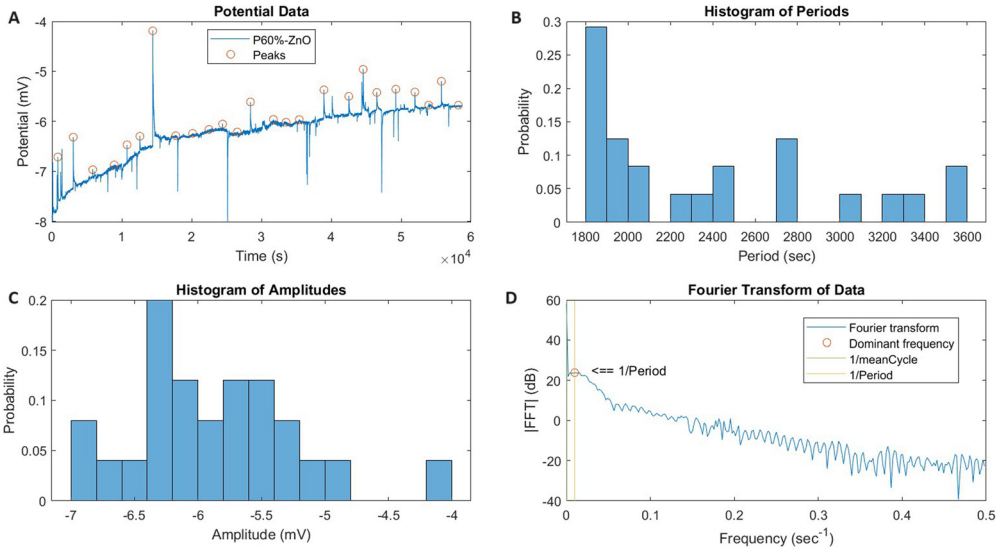

Fig. 11 Electrical spiking activity of 60 : 40% L-Glu : L-Arg : ZnO colloidal nanoparticles after visible light irradiation. The colloidal nanoparticles composed of L-Glu : L-Arg, and ZnO were subjected to visible light irradiation. The electrical potential exhibits oscillatory spiking behaviour over time. Transient electrical potential *versus* time exhibits oscillatory spiking behaviour, according to (A). (B) Histogram of inter-spike interval durations, with a mean period of 2400 ± 600 seconds. (C) Histogram of spike amplitude potentials, averaging −5.9 ± 0.6 mV. (D) Analysis of the Fourier transform reveals a dominant frequency component at 0.042 Hz, which corresponds to the average spiking period. The data demonstrate that this proteinoid–inorganic composite retains its electrical excitability and "memory" of prior illumination. The emergent spiking dynamics resemble aspects of neural systems, highlighting the potential for these materials to be utilised in brain-inspired computation.

research is focused on understanding the molecular basis of spiking phenomena in order to advance the field of bioelectronics.[68] The neuromorphic potential of the 30 : 70% L-Glu : L-Arg : ZnO bio-nano composite is highlighted by the appearance of rhythmic electrical spiking activity, as shown in Fig. 13. The electrical response initially remained stable for more than 26 000 seconds before shifting into an oscillatory pattern. This implies the existence of long-lasting photomemory effects, where previous exposure to light is remembered through the activation of connected excitable states.

The electrical potential signals exhibited characteristic spiking patterns. To quantify the spike timing statistics, the spike rate was calculated based on the intervals between detected spike peaks as follows:

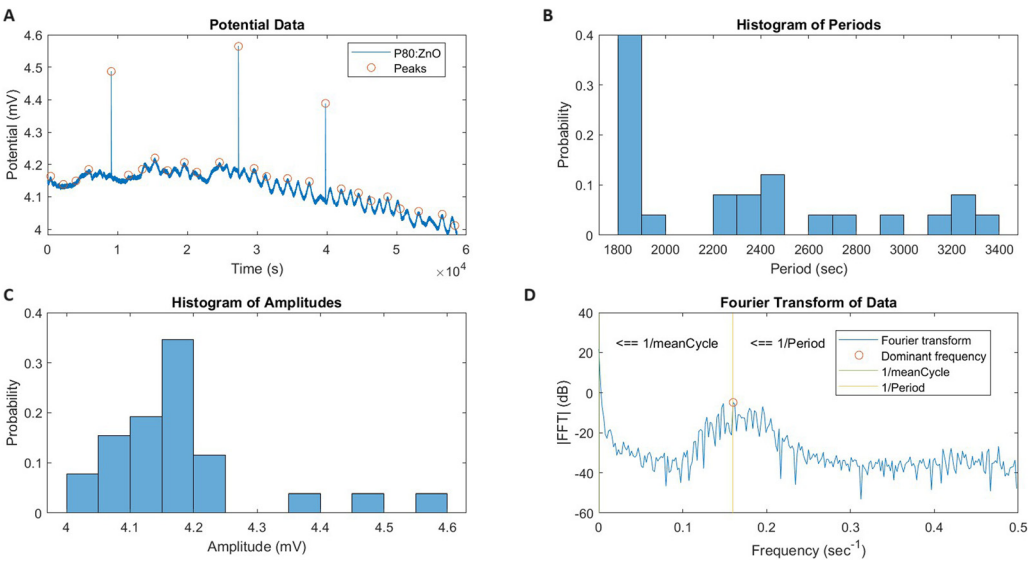

Fig. 12 Spiking photomemory dynamics of 80 : 20% L-Glu : L-Arg : ZnO colloidal nanoparticles after visible light exposure. (A) The transient response exhibits oscillatory electrical potential spikes. (B) The mean period of the spike intervals is 2300 ± 500 s. (C) The average spike amplitude potential is 4.18 ± 0.13 mV. (D) The mean spiking period is matched by the Fourier transform's dominant frequency of 0.043 Hz. The proteinoid–inorganic combination has spectral memory effects and long-term excitability that resemble brain processes. The findings point to possible methods for employing these programmable bio-nano materials to achieve learning and signal processing abilities inspired by the brain.

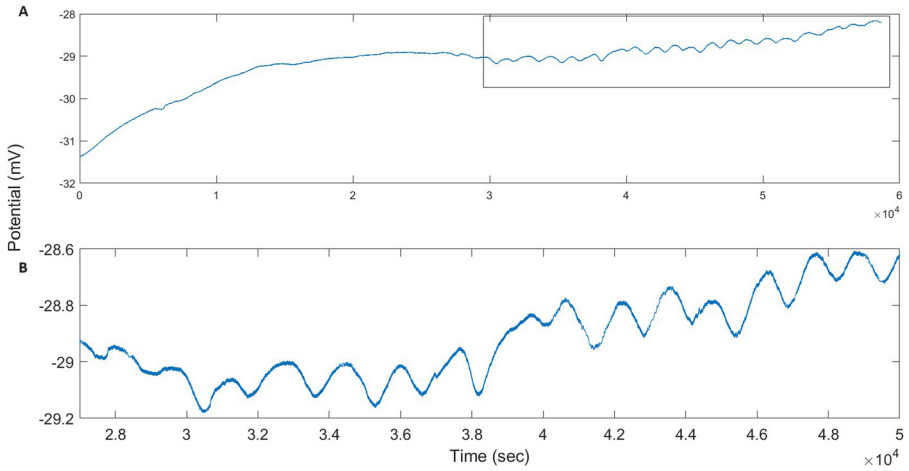

Fig. 13 Electrical potential dynamics of a 30 : 70% L-Glu : L-Arg : ZnO proteinoid–inorganic nanocomposite, exhibiting spiking oscillations emerging after 26 264 s post-illumination. The transition from a quiescent to an electrically active spiking regime exhibits long-lasting ''photomemory'' effects, where the material remembers previous exposure to visible light stimuli. The potential of programmable bio-nano soft materials for light-addressable unconventional computing applications is highlighted by their ability to trigger and modulate neural-like emergent behaviours through light irradiation.

$$T_i = l_{i+1} - l_i \quad (1)$$

where T_i is the inter-spike interval between successive peaks located at l_i and l_{i+1}. The instantaneous spike rate R_i measured in Hertz was then computed as:

$$R_i = \frac{1}{T_i} = \frac{1}{l_{i+1} - l_i} \quad (2)$$

This derives the spike rate in Hz from the time differences between spikes. Analysis of the rate provides insight into the dynamics of the spiking activity.

The analysis of the spike rate evolution (Fig. 14) showed a gradual increase from 0 to approximately 0.50 Hz as the material adapted over time. The spatio-temporal pattern bears resemblance to the firing patterns observed in complex biological neural networks.

These results demonstrate the diverse and complex dynamics that can be achieved by adjusting the composition of these programmable soft matter systems. The proteinoid–inorganic components work together in a cooperative manner to imitate certain aspects of brain physiology. These aspects include memory, spike timing adaptation, and learning that resembles neural networks. By further developing and integrating these photo-responsive elements, it is possible to achieve revolutionary brain-inspired computer architectures.

3.4. Photocurrent amplification *via* light intensity programming

The photo-response of proteinoid–ZnO was analysed to determine its dependence on intensity. This analysis was conducted

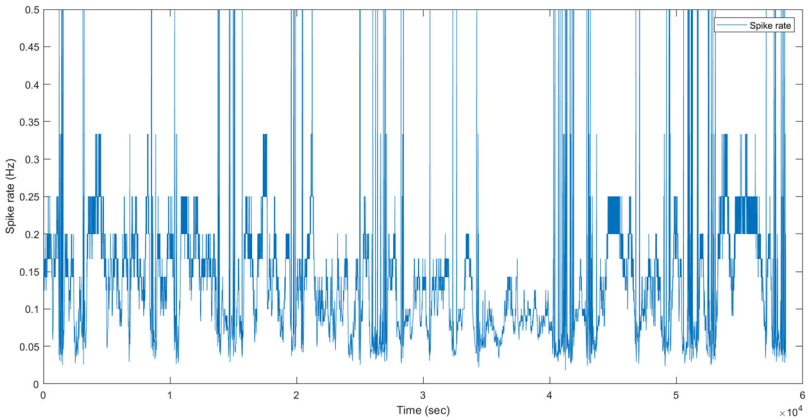

Fig. 14 The spike rate dynamics of a 30 : 70% ratio. The study investigates the behaviour of the L-Glu : L-Arg : ZnO proteinoid–ZnO nanocomposite over time after illumination. Following a period of inactivity, there is a noticeable increase in oscillatory spiking activity, with spike rates reaching approximately 0.5 Hz. The increase in spiking frequency over time indicates that the coupled states are becoming more excited and that the activation kinetics of the bio-nano composite are becoming more complex. The analysis of changes in spike rate over time and space helps us understand how metastable states are formed through interactions between light, proteinoids, and inorganic substances. The programmable neuromorphic response showcased in this study highlights the potential for creating adaptive brain-inspired behaviours through engineering.

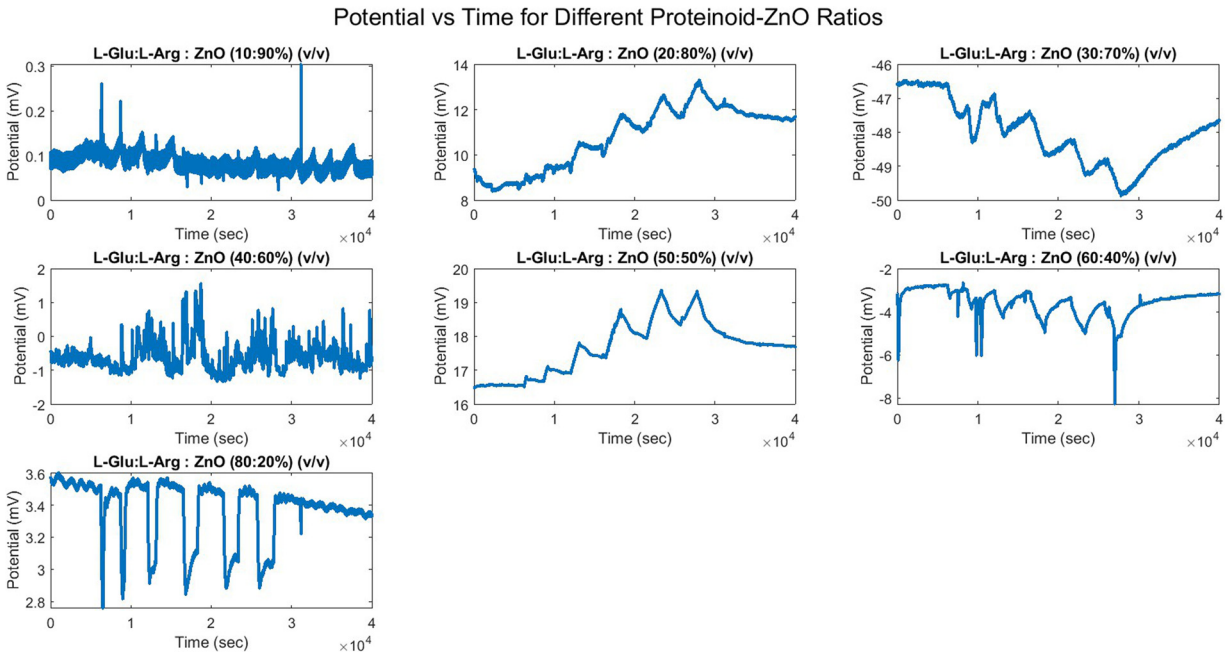

Fig. 15 The modulation of proteinoid–inorganic photoresponse can be achieved by adjusting the intensity of daylight. Bio-nano composites of L-Glu : L-Arg : ZnO with proteinoid ratios ranging from 10% to 80% were subjected to irradiation using low (25%), medium (50%), and high (100%) intensity visible daylight. The profiles of transient electrical potentials show that there are intensity-dependent effects on the generation of photo-current, the kinetics of oscillation, and the emergence of spiking behaviours. Lower light power densities lead to delayed emergence and decreased amplitudes of the photo-response. The results demonstrate that the amplification of proteinoid–inorganic interactions can be adjusted by controlling the intensity of the input light. The focus of future research is to enhance the materials' ability to respond to changes in ambient lighting conditions, specifically for adaptive technologies.

by examining a range of compositional ratios, as shown in Fig. 16. The use of cubic polynomial fits to analyse the response-illuminance data allowed for a sensitivity analysis, which helped quantify the light modulation efficiency for each mixture. The formulation with a ratio of 20 : 80 demonstrated the highest sensitivity, measuring at 1.4×10^{-6} mV per lux. This indicates that it achieved an ideal combination of proteinoid-mediated enhancement and inorganic photo-

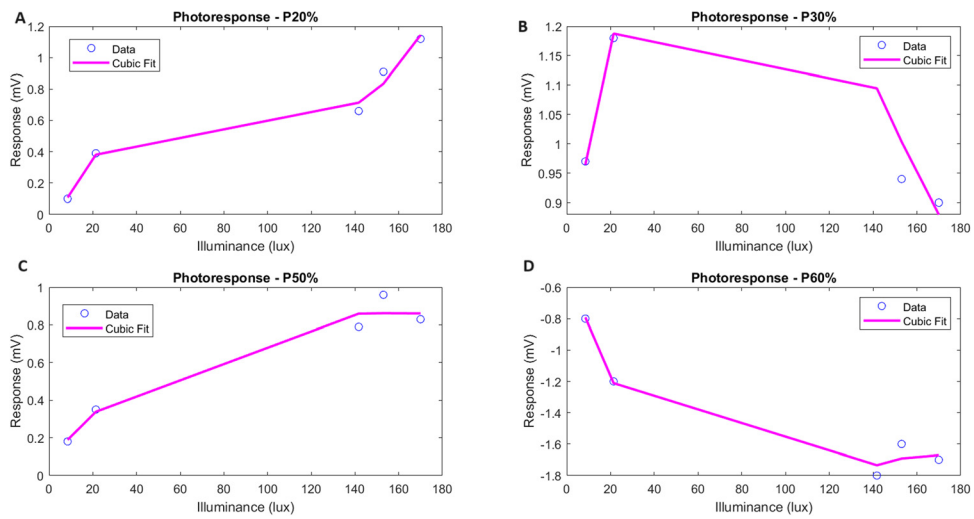

Fig. 16 Sensitivity of L-Glu : L-Arg : ZnO nanoparticles to light as a function of their proteinoid content. For the compositional ratios of (A) 20 : 80, (B) 30 : 70, (C) 50 : 50, and (D) 60 : 40% v/v proteinoid to ZnO, the illumination intensity-dependent response was fitted with a cubic polynomial. According to the cubic fit coefficients, the estimated sensitivities for 20 : 80, 30 : 70, 50 : 50, and 60 : 40% are 1.4×10^{-6}, 5.6×10^{-7}, 1.6×10^{-7}, and -1.0×10^{-6} mV per lux, respectively. Maximum sensitivity is obtained at a ratio of 2 : 8 proteinoid to ZnO, highlighting the photo-conduction enhancement mediated by proteinoid. The nonlinear relationships highlight the complex relationship between light intensity and emergent proteinoid–inorganic photo-response behaviours.

Table 3 Photo-response sensitivity of L-Glu : L-Arg : ZnO colloidal nanoparticles

Composition (% v/v)	*R*-squared	Sensitivity (mV per lux)
P20%ZnO	0.85	1.4×10^{-6}
P30%ZnO	−0.29	5.6×10^{-7}
P50%ZnO	0.73	1.6×10^{-7}
P60%ZnO	0.83	-1.0×10^{-6}

response. When the proteinoid percentages were lower, there was a decrease in photo-current generation, which suggests that there were reduced interfacial effects. However, when the proteinoid content exceeds the optimal ratio, there is a decline in the photo-response, eventually leading to its inversion. This suggests that there are complex synergistic interactions that are responsible for the emergence of light-triggered behaviours. Additional mechanistic studies are being conducted to clarify the impact of proteinoid density and conformational effects. In general, the relationships between intensities demonstrate the ability to adjust photo-sensitivity by programming the composition. This establishes the basis for customising bio-nano hybrids in a logical manner, allowing them to be used in optical information processing and unconventional computing devices guided by light.

The photo-response of proteinoid–ZnO was analysed across various compositions to determine its dependence on light intensity. The results of this analysis are summarised in Table 3. The maximum sensitivity of 1.4×10^{-6} mV per lux is achieved with a proteinoid ratio of 20%. This indicates that there is optimal interfacial coupling at this particular ratio. The observed negative sensitivity of -1.0×10^{-6} mV per lux for the 60% mixture suggests that there is an inversion of the photo-response curve when there is a higher proteinoid content.

This inversion can be attributed to the increase in charge-carrier recombination and exciton decay rates, which are mediated by proteinoid–proteinoid interactions. At higher densities of proteinoids, the dynamics of excitation are primarily influenced by intramolecular relaxation rather than charge separation.

The tunability of the photo-response characteristics is demonstrated by the compositional programming of the proteinoid–ZnO systems. Fig. 17 demonstrates that when the proteinoid to inorganic ratio was 80 : 20%, the response reached saturation at higher illumination intensities. This is in contrast to the continuous increase observed for other mixtures. This suggests that there is an emergent constraint on the capacity to harvest light, which is connected to the high density of proteinoids.

The presence of nonlinear sensitivity in photo-detectors or sensing applications indicates the possibility of distinguishing between low and high intensity stimuli. Fig. 18 provides additional characterization of the complex dynamic behaviours through the utilisation of Fourier and time-frequency analysis techniques. The spectral decomposition allows us to identify the important oscillatory modes, while the scalogram shows how these modes change over time.

These results provide insight into how the magnitude and kinetics of the photo-response can be customised through synthetic biomolecular engineering. The ability to adjust sensitivity, tuning ranges, and emergent spatiotemporal patterns holds great potential for developing optical logic and establishing the ba-sis for computing with dynamic proteinoid materials. Ongoing efforts are currently being directed towards establishing a connection between composition and photophysics in order to advance the field of bio-inspired information processing.

4. Discussion

The proteinoid–ZnO composites have distinct photo-sensitivity signatures, which allows for optical differentiation of proteinoid content. This is illustrated through the optical mapping

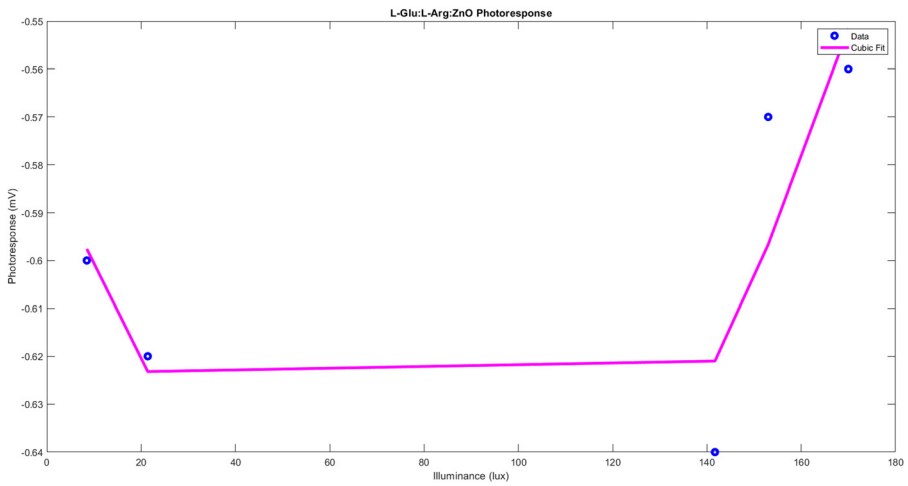

Fig. 17 The photoresponse of colloidal nanoparticles composed of L-Glu, L-Arg, and ZnO with a proteinoid ratio of 80 : 20% v/v demonstrates saturation behaviour when exposed to increasing levels of visible light irradiation. The electrical potential response exhibits a plateau at greater light intensities, in contrast to the continuous increase reported in other compositions. This suggests that the proteinoid-rich combination reaches a point of saturation in terms of photo-active centres when exposed to high levels of illumination. The integration of nonlinear sensitivity in optical sensing systems has the potential to enhance selectivity and enable customizable spectrum discrimination.

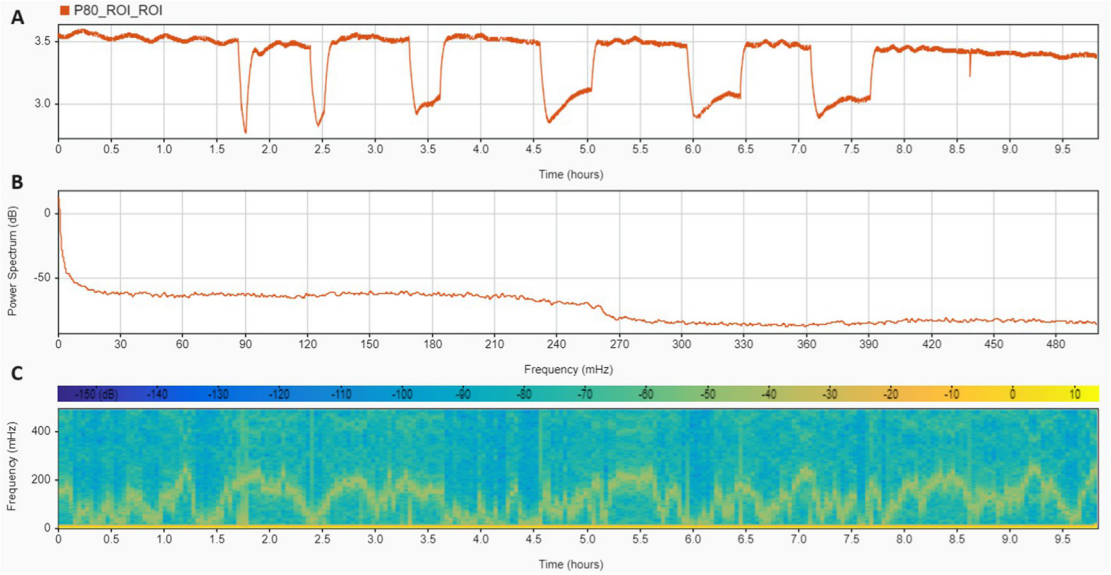

Fig. 18 (A) Electrical potential dynamics of an 80 : 20 percent mixture nanocomposite of L-Glu : L-Arg : ZnO proteinoid and inorganic compound. (B) The transient photo-current response measured over 48 hours demonstrates oscillations. The promi-nent frequency components of the oscillations are revealed by Fourier transform analysis. (C) The time-frequency distribution is depicted by the scalogram computed by continuous wavelet transform, indicating variations in oscillation periods over the timescale. These hybrid smart materials exhibit complex oscillatory behaviours as a consequence of the interfacial interactions between the biological and inorganic components. Relationships between dynamic photo-responses and tunable material prop-erties for unconventional computing applications are the subject of ongoing research.

presented in Fig. 21. Distinct spectral barcodes are generated for each formulation by encoding the normalised sensitivity values into binary reflectance states.

Fig. 23 illustrates how the proteinoid–ZnO mixture can absorb light in the visible spectrum and generate electrons and holes that can participate in chemical reactions. An analytical calculation of the energy gaps (E_g) of ZnO nanoparticles and proteinoid microspheres can be found in the supplementary material. This is relevant to our research question, as we aim to investigate the effect of light intensity and wave-length on the reaction rate and product yield of the proteinoid–ZnO mixture.The Fig. 23 shows that the proteinoid–ZnO mixture can act as a photo-catalyst for various organic synthesis reactions. The Fig. 23 illustrates the synergistic system of proteinoid–ZnO, which offers a means to augment photo-sensitivity by leveraging the complementary characteristics of the biological and inorganic constituents. Proteinoids possess desirable characteristics such as processability, structural flexibility, and biocompatibility.[36,69,70] In addition, the ZnO nanoparticles exhibit redox activity, possess surface electronic states, and demonstrate effective light absorption.[8,71,72] Tunable optoelectronic capabilities arise from the tailored intermolecular and interfacial interactions through the integration of various parts in a basic self-assembly process. Systematic variation of composition and illumination conditions presents possibilities for deliberate manipulation of photo-conductive pathways. The examination of the mechanisms that underlie the collaborative reaction is essential in order to comprehend the structural and functional basis of the photo-sensitization phenomena.[73] The observed spectral sensitivity is most likely a result of the photoexcitation of ZnO, which leads to the injection of charges into proteinoid orbitals. This process is facilitated by the close integration between the two components. The morphology and structure of proteinoids subsequently impact the kinetics and transport of excitons.

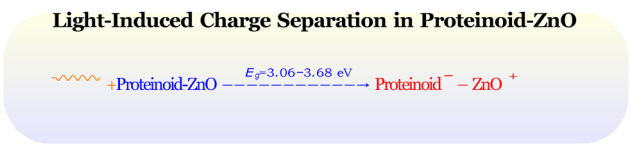

Fig. 19 Schematic representation of light-induced charge separation in proteinoid–ZnO complexes, showing the energy gap range (E_g) for various wavelengths of light. Daylight and grey are polychromatic radiations, consisting of a broad spectrum of wavelengths in the visible range.

The HOMO is the highest energy molecular orbital that is occupied by electrons in the ground state of a molecule. It is represented by the eigenfunction ψ_{HOMO} and eigenvalue ε_{HOMO} obtained from the solution of the Schrödinger equation:

$$\hat{H}\psi_{HOMO} = \varepsilon_{HOMO}\psi_{HOMO} \quad (3)$$

where $\hat{H}$ is the Hamiltonian operator describing the total energy of the system.

The HOMO plays a crucial role in chemical reactivity and determines the ionization potential (IP) of the molecule:

$$IP = -\varepsilon_{HOMO} \quad (4)$$

The LUMO is the lowest energy molecular orbital that is unoccupied by electrons in the ground state of a molecule. It is represented by the eigenfunction ψ_{LUMO} and eigenvalue ε_{LUMO} obtained from the solution of the Schrödinger equation:

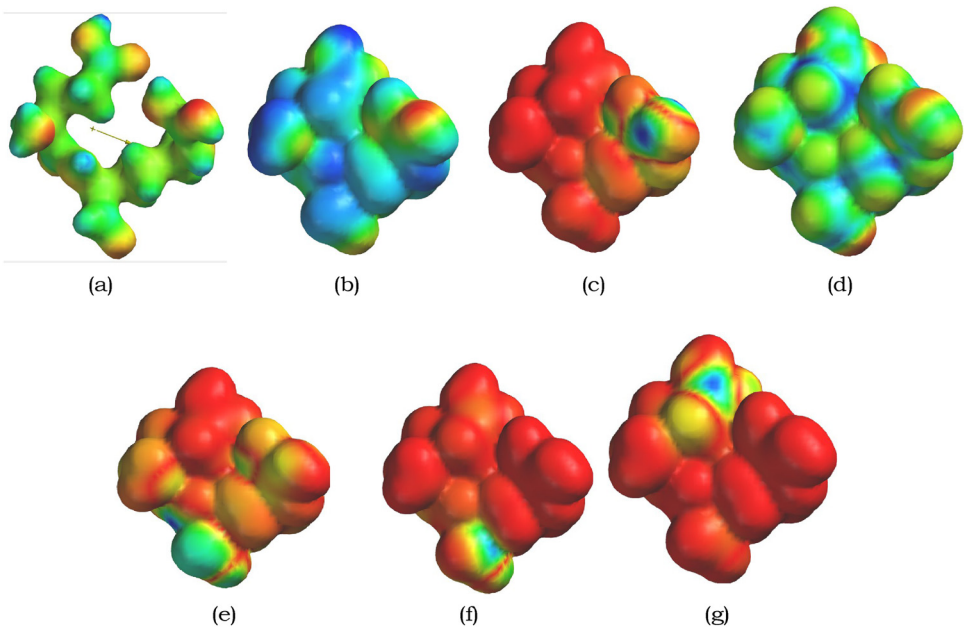

Fig. 20 Density potential diagrams of L-Glu : L-Arg proteinoids generated using the AVOGADRO computational program. (a) The density potential with an arrow indicating the dipole moment. (b) The density potential of the charged proteinoid. (c) The density potential during ionization. (d) The density potential of the highest occupied molecular orbital minus one (HOMO−1). (e) The density potential of the lowest unoccupied molecular orbital plus one (LUMO+1). (f) The density potential of the highest occupied molecular orbital (HOMO). (g) The density potential of the lowest unoccupied molecular orbital (LUMO). The colour scale represents the electronegativity of the proteinoids, with green indicating the lowest electronegativity, followed by blue, yellow, and red representing the highest electronegativity. These diagrams provide insights into the electronic structure and charge distribution of the L-Glu : L-Arg proteinoids, revealing the dipole moment, charge distribution in the charged state, ionization behaviour, and the characteristics of the HOMO−1, LUMO+1, HOMO, and LUMO orbitals. The varying electronegativity levels across the proteinoid structure suggest the presence of charge asymmetry and potential reactive sites, which may play a role in the chemical and biological properties of these molecules.

$$\hat{H}\,\psi_{\mathrm{LUMO}} = \varepsilon_{\mathrm{LUMO}}\psi_{\mathrm{LUMO}} \tag{5}$$

where $\hat{H}$ is the Hamiltonian operator describing the total energy of the system.

The LUMO plays a significant role in chemical reactivity and determines the electron affinity (EA) of the molecule:

$$\mathrm{EA} = -\varepsilon_{\mathrm{LUMO}} \tag{6}$$

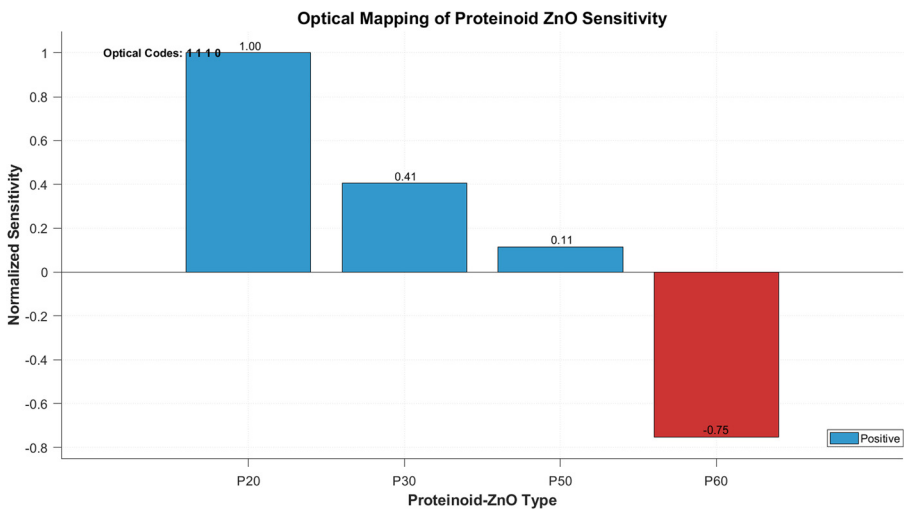

Fig. 21 Proteinoid–ZnO nanocomposite photo-sensitivity optical mapping. The optical reflectance signals encode the nor-malised sensitivity values for compositions with 20%, 30%, 50%, and 60% proteinoid ratio. Positive sensitivity corresponds to a reflective state, whereas negative sensitivity corresponds to a nonreflective state. This provides a spectral signature for distinguishing the proteinoid content based on the intensity-dependent photo-response to illumination. Further development of the mapping method could enable optical measurement of the properties of bio-nano composite materials for applications involving optical sensing.

The energy difference between the HOMO and LUMO, known as the HOMO–LUMO gap ($\Delta E_{\text{HOMO–LUMO}}$), is an important parameter that influences the electronic and optical properties of molecules:

$$\Delta E_{\text{HOMO–LUMO}} = \varepsilon_{\text{LUMO}} - \varepsilon_{\text{HOMO}} \quad (7)$$

The synergistic effects between proteinoids and ZnO occur due to the photo-excitation of interfacial charge transfer states. This is illustrated in the chemical reactions below. The excitation of electrons from proteinoid orbitals to the ZnO conduction band occurs when photons are absorbed across the visible spectrum. This results in the formation of localised positive holes on the proteinoid chains.

The spectral shift of the effective bandgap (E_g) suggests that the density of interfacial electronic states can be modulated by the wavelength of the incident light. Under blue light, the presence of a greater number of mid-gap states results in the ability to undergo transitions at a lower photon energy of 3.1 eV, as opposed to the higher photon energy of 3.3 eV required under daylight conditions. The broad spectral photosensitization can be explained by the proteinoid-mediated band structure engineering. The E_g values are calculated in the supplementary material (Fig. 19).

Ongoing studies in spectro-electrochemistry are focused on quantifying the changes in band positions that occur due to light and establishing a correlation between the interfacial density of states and the proteinoid conformation.[74,75] By elucidating the relationships between structure and property, we can uncover design principles that will allow us to engineer emergent optoelectronic phenomena. This programming can be applied to bio-inspired computing and adaptive electronics applications. Fig. 19 presents a schematic representation of light-induced charge separation in proteinoid–ZnO complexes. The energy gap range (E_g) for various wavelengths of light is shown, indicating the potential for charge separation upon light absorption.

The electronic structure and charge distribution of the L-Glu : L-Arg proteinoids were studied using the AVOGADRO computational program.[76] Fig. 20 presents the density potential diagrams obtained from these calculations. The density potential diagram with an arrow (Fig. 20a) reveals the dipole moment of the proteinoid, indicating the presence of charge asymmetry within the molecule. The charged state of the proteinoid (Fig. 20b) showcases the charge distribution, highlighting the regions of positive and negative charge. The ionization behaviour of the proteinoid is depicted in Fig. 20c, providing insights into the electron density changes during the ionization process. The density potential diagrams of the HOMO−1 and LUMO+1 orbitals (Fig. 20d and e, respectively) reveal the spatial distribution of these important molecular orbitals, which play a role in the chemical reactivity and electronic transitions of the proteinoid. The colour scale in the density potential diagrams represents the electronegativity of the proteinoid, with green indicating the lowest electronegativity and red representing the highest. The varying electronegativity levels across the proteinoid structure suggest the presence of potential reactive sites and charge asymmetry, which may contribute to the unique chemical and biological properties of the L-Glu : L-Arg proteinoids.

The photon energy, denoted as $h\nu$, represents the energy of a photon. The effective bandgap, represented by E_g, refers to the energy difference between the highest occupied energy levels of the proteinoid and the conduction band edge of the ZnO nanoparticles. The arrows indicate the excitation of an electron from the highest occupied energy levels of the proteinoid to the conduction band of the ZnO. For the proteinoid component, we can still refer to its highest occupied molecular orbital (HOMO), while for the ZnO nanoparticles, we use the terminology of valence band maximum (VBM) and conduction band minimum (CBM) to describe its electronic structure.

The various colours of light contain enough photon energy to bridge the gap between proteinoid and ZnO, resulting in the formation of charge separated states and the generation of photo-current. The variation in bandgap is caused by the adjustable density of interfacial electronic states in response to different wavelengths of illumination.[77–81]

The proteinoid samples with positive sensitivity, specifically the 20%, 30%, and 50% samples, are associated with reflective optical signals. On the other hand, the 60% sample, which has negative sensitivity, corresponds to a non-reflective state. The set of nanocomposite compositions is optically coded as [1 1 1 0].

The use of optical readout for spectral barcodes enables quick identification of properties and functionalities of bio-nano materials solely through light–matter interactions. The use of light to encode various forms of information, including but not limited to position, speed, direction, or data, is known as optical encoding. Optical encoding can be accomplished through a range of techniques, including the use of optical fibers, holography, photonic crystals, plasmonic nanostructures, or quantum dots. The structure–property origins of optical encoding

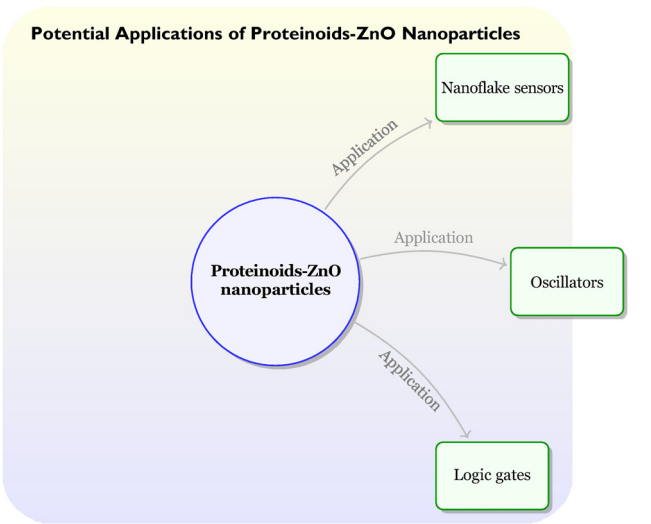

Fig. 22 Schematic representation of potential applications for proteinoids–ZnO nanoparticles in unconventional computing devices, including nanoflake sensors, oscillators, and logic gates.

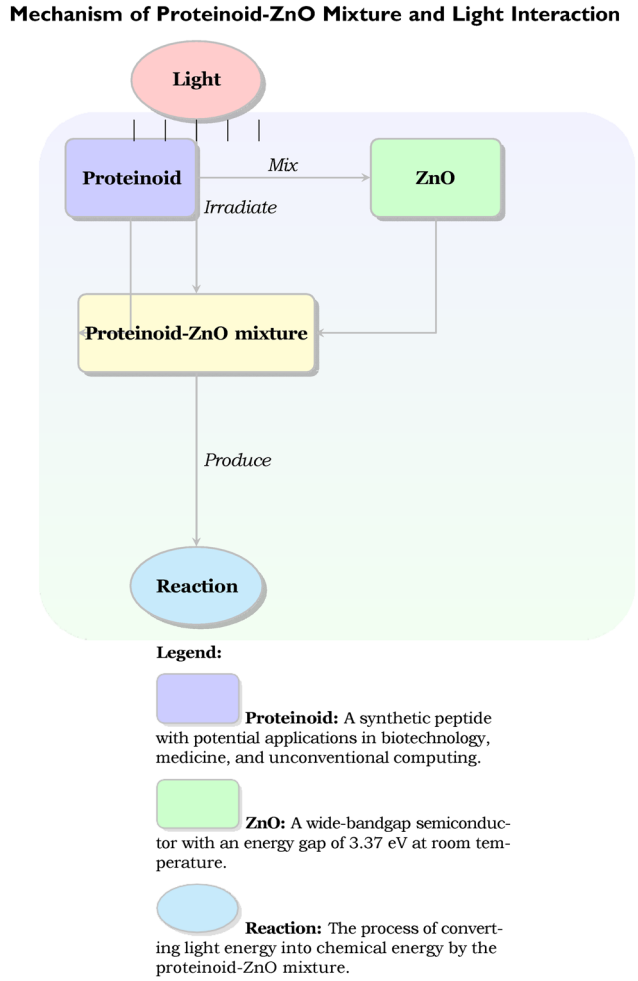

Fig. 23 A schematic diagram illustrating the mechanism of interaction between the proteinoid–ZnO mixture and light of different colors.

pertain to the correlation between the physical and chemical attributes of materials and devices employed in optical encoding, and their resultant optical performance and functionality.[82,83]

Current efforts are dedicated to the development of protocols for programming proteinoid photo-sensitivity through synthetic tailoring. Additionally, researchers are working on understanding the structure–property origins of the optical encoding.[84,85] The ability to use intrinsic photo-responses to optically probe, differentiate, and classify the emergent behaviours of proteinoids offers a promising approach to achieve highly parallel bio-inspired optical computing.

The proteinoids–ZnO nanocomposites exhibit strong photo-responses when exposed to visible light, indicating their potential usefulness in emerging computational frameworks. The hybrid systems shown in Fig. 6 exhibit a tailored spectral sensitivity, oscillatory current outputs, and dynamic photo-conductivity. These characteristics indicate that these systems have the potential to be used as fundamental components in bio-inspired, brain-like ''proteinoid computer'' architectures.

The oscillatory photo-current profiles, which have rapid recovery kinetics, are particularly suitable for implementing oscillators and clock signals. Furthermore, the binary photo-response behaviour has the potential to aid in the development of logic gates used for fundamental Boolean operations. By further exploring compositional tuning, we can expand spectral and amplitude discrimination, which in turn could enable the use of multi-valued logic encodings.

In addition, the composite nanocomposite structure is highly suitable for applications in high-sensitivity photo-detectors. Nanoflake-like networks of photo-responsive colloids, when further developed, have the potential to serve as sensors for optical pattern recognition in proteinoid neural networks.

In summary, proteinoids–nanoparticle hybrids offer a promising materials platform for developing unconventional computing technologies inspired by the human brain. By emulating aspects of natural neuronal systems and harnessing light–matter interactions, these hybrids have the potential to revolutionise brain-inspired computing.

5. Conclusion

This study examines the photo-response of proteinoid–ZnO colloidal nanoparticles when exposed to visible light irradiation. It has been observed that the photo-response is reliant upon both the composition of the proteinoid–ZnO mixture and the intensity of the incident light. The study has provided evidence indi-cating the existence of a trade-off relationship between the sensitivity and stability of the photo-response. Additionally, it has been determined that an ideal proteinoid ratio of 20% yields maximum sensitivity. An intriguing phenomenon of photo-response inversion has been reported in conditions where the proteinoid content exceeds 60%. This observation implies that distinct methods of photo-induced charge transfer occur at various interactions between proteinoids and ZnO. The results of our study offer novel perspectives on the photo-physical characteristics of proteinoid–ZnO nanoparticles and their prospective utilisation in optoelectronic devices (Fig. 22).

Data availability

The data is available on the Zenodo site at the following link: **https://zenodo.org/records/12698081**.

Conflicts of interest

There are no conflicts to declare.

Acknowledgements

PM was supported by EPSRC Grant EP/W010887/1. NRK was supported by funding from the EC Pathfinder Open grant No. 964388. Authors are grateful to David Paton for helping with SEM imaging and to Neil Phillips for helping with instruments.

References

1 E. McGlynn, M. O. Henry and J.-P. Mosnier, ZnO wide-bandgap semiconductor nanostructures: Growth, *Characterization, and Applications*, 2010, pp. 523–571.
2 S. Raha and M. Ahmaruzzaman, Zno nanostructured materials and their potential applications: progress, challenges and perspectives, *Nanoscale Adv.*, 2022, **4**(8), 1868–1925.
3 S. Singh, T. Chaudhary and G. Khanna, Recent advancements in wide band semiconductors (sic and gan) technology for future devices, *Silicon*, 2022, **14**(11), 5793–5800.
4 N. R. Kheirabadi, A. Chiolerio, N. Phillips and A. Adamatzky, Learning in colloids: Synapse-like zno+ dmso colloid, *Neurocomputing*, 2023, **557**, 126710.
5 P. Uikey and K. Vishwakarma, Review of zinc oxide (zno) nanoparticles applications and properties, *Int. J. Emerg. Technol. Comput. Sci. Electron.*, 2016, **21**(2), 239–242.
6 Z.-Y. Zhang and H.-M. Xiong, Photoluminescent zno nanoparticles and their biological applications, *Materials*, 2015, **8**(6), 3101–3127.
7 M. A. Desai and S. D. Sartale, Plasmonic metal nanoparticles decorated zno nanostructures for photo-electrochemical (pec) applications, *Chemically Deposited Nanocrystalline Metal Oxide Thin Films: Synthesis, Characterizations, and Applications*, Springer, 2021, pp. 293–328.
8 S. Baruah, S. S. Sinha, B. Ghosh, S. K. Pal, A. Raychaudhuri and J. Dutta, Photoreactivity of ZnO nanoparticles in visible light: Effect of surface states on electron transfer reaction, *J. Appl. Phys.*, 2009, **105**(7), 074308.
9 D. B. Potter, M. J. Powell, I. P. Parkin and C. J. Carmalt, Aluminium/gallium, indium/gallium, and aluminium/indium co-doped zno thin films deposited via aerosol assisted cvd, *J. Mater. Chem. C*, 2018, **6**(3), 588–597.
10 S. H. Khan, B. Pathak and M. Fulekar, A study on the influence of metal (fe, bi, and ag) doping on structural, optical, and antimicrobial activity of zno nanostructures, *Adv. Compos. Hybrid Mater.*, 2020, **3**, 551–569.
11 A. Dhupar, S. Kumar, H. S. Tuli, A. K. Sharma, V. Sharma and J. K. Sharma, In-doped zns nanoparticles: structural, morphological, optical and antibacterial properties, *Appl. Phys. A*, 2021, **127**, 1–11.
12 Z. Kang, H. Si, S. Zhang, J. Wu, Y. Sun, Q. Liao, Z. Zhang and Y. Zhang, Interface engineering for modulation of charge carrier behavior in zno photoelectrochemical water splitting, *Adv. Funct. Mater.*, 2019, **29**(15), 1808032.
13 A. Wolcott, W. A. Smith, T. R. Kuykendall, Y. Zhao and J. Z. Zhang, Photoelectrochemical study of nanostructured zno thin films for hydrogen generation from water splitting, *Adv. Funct. Mater.*, 2009, **19**(12), 1849–1856.
14 A. Tauffenberger and P. J. Magistretti, Reactive oxygen species: beyond their reactive behavior, *Neurochem. Res.*, 2021, **46**, 77–87.
15 Z. He, Q. Xu, B. Newland, R. Foley, I. Lara-Sáez, J. F. Curtin and W. Wang, Reactive oxygen species (ros): utilizing injectable antioxidative hydrogels and ros-producing therapies to manage the double-edged sword, *J. Mater. Chem. B*, 2021, **9**(32), 6326–6346.
16 S. Sachdev, S. A. Ansari and M. I. Ansari, Reactive oxygen species (ros): An introduction, *Reactive Oxygen Species in Plants: The Right Balance*, Springer, 2023, pp. 1–22.
17 D. Chen, Y. Cheng, N. Zhou, P. Chen, Y. Wang, K. Li, S. Huo, P. Cheng, P. Peng and R. Zhang, *et al.*, Photocatalytic degradation of organic pollutants using tio2-based photocatalysts: A review, *J. Cleaner Prod.*, 2020, **268**, 121725.
18 E. A. S. Dimapilis, C.-S. Hsu, R. M. O. Mendoza and M.-C. Lu, Zinc oxide nanoparticles for water disin-fection, *Sustainable Environ. Res.*, 2018, **28**(2), 47–56.
19 S. H. Khan and B. Pathak, Zinc oxide based photocatalytic degradation of persistent pesticides: A com-prehensive review, *Environ. Nanotechnol., Monit. Manage.*, 2020, **13**, 100290.
20 N. Raeisi Kheirabadi, A. Chiolerio and A. Adamatzky, Pavlovian reflex in colloids, *Bionanoscience*, 2024, 1–9.
21 N. Roberts, N. Raeisi Kheirabadi, M.-A. Tsompanas, A. Chiolerio, M. Crepaldi and A. Adamatzky, Logical circuits in colloids, *R. Soc. Open Sci.*, 2024, **11**(5), 231939.
22 M. Ahmad, J. Zhao, J. Iqbal, W. Miao, L. Xie, R. Mo and J. Zhu, Conductivity enhancement by slight indium doping in zno nanowires for optoelectronic applications, *J. Phys. D: Appl. Phys.*, 2009, **42**(16), 165406.
23 D. Gao, Z. Zhang, J. Fu, Y. Xu, J. Qi and D. Xue, Room temperature ferromagnetism of pure ZnO nanoparticles, *J. Appl. Phys.*, 2009, **105**(11), 113928.
24 Z. L. Wang and J. Song, Piezoelectric nanogenerators based on zinc oxide nanowire arrays, *Science*, 2006, **312**(5771), 242–246.
25 S. Sulaiman, I. Sudin, U. M. B. Al-Naib and M. F. Omar, Review of the nanostructuring and doping strategies for high-performance zno thermoelectric materials, *Crystals*, 2022, **12**(8), 1076.
26 P. Mougkogiannis, N. Raeisi Kheirabadi, A. Chiolerio and A. Adamatzky, Electrical spiking activity of proteinoids–ZnO colloids, *Neuromorphic Computing and Engineering*, 2023, **4**(1), 014007.
27 R. Fortulan, N. R. Kheirabadi, P. Mougkogiannis, A. Chiolerio and A. Adamatzky, Reservoir computing with colloidal mixtures of zno and proteinoids, *arXiv*, 2023, preprint, arXiv:2312.08130, DOI: **10.48550/arXiv.2312.08130**.
28 R. A. C. Ferraz, A. L. G. Lopes, J. A. F. da Silva, D. F. V. Moreira, M. J. N. Ferreira and S. V. de Almeida Coimbra, Dna–protein interaction studies: a historical and comparative analysis, *Plant Methods*, 2021, **17**(1), 1–21.
29 S. W. Fox, J. R. Jungck and T. Nakashima, From proteinoid microsphere to contemporary cell: formation of internucleotide and peptide bonds by proteinoid particles, *Origins Life*, 1974, **5**, 227–237.
30 S. W. Fox, K. Harada and J. Kendrick, Production of spherules from synthetic proteinoid and hot water, *Science*, 1959, **129**(3357), 1221–1223.
31 S. Sharma, A. Mahmud, G. Tarabella, P. Mougoyannis and A. Adamatzky, On morphological and functional complexity of proteinoid microspheres, *arXiv*, 2023, preprint, arXiv:2306.11458, DOI: **10.48550/arXiv.2306.11458**.

32 M. Rodriguez Garcia, *Engineering the transition from non-living to living matter*, PhD thesis, University of Glasgow, 2016.
33 S. W. Fox, T. Nakashima, A. Przybylski and R. M. Syren, The updated experimental proteinoid model, *Int. J. Quantum Chem.*, 1982, **22**(S9), 195–204.
34 S. W. Fox and K. Harada, Thermal copolymerization of amino acids to a product resembling protein, *Science*, 1958, **128**(3333), 1214.
35 D. L. Rohlfing, Thermal polyamino acids: synthesis at less than 100 c, *Science*, 1976, **193**(4247), 68–70.
36 P. Mougkogiannis, N. Phillips and A. Adamatzky, Transfer functions of proteinoid microspheres, *Biosystems*, 2023, **227**, 104892.
37 T. Nakashima and S. Fox, Synthesis of peptides from amino acids and atp with lysine-rich proteinoid, *J. Mol. Evol.*, 1980, **15**, 161–168.
38 K. Matsuno, Natural self-organization of polynucleotides and polypeptides in protobiogenesis: appear-ance of a protohypercycle, *BioSystems*, 1982, **15**(1), 1–11.
39 N. Guttenberg, N. Virgo, K. Chandru, C. Scharf and I. Mamajanov, Bulk measurements of messy chemistries are needed for a theory of the origins of life, *Philos. Trans. R. Soc., A*, 2017, **375**(2109), 20160347.
40 A. Adamatzky, Towards proteinoid computers. hypothesis paper, *BioSystems*, 2021, **208**, 104480.
41 P. L. Gentili, The fuzziness of the molecular world and its perspectives, *Molecules*, 2018, **23**(8), 2074.
42 C. A. Lindley, Synthetic intelligence: beyond artificial intelligence and robotics, *Integr. Biomathics: Tracing Road Reality*, 2012, 195–204.
43 E. Bonabeau, M. Dorigo and G. Theraulaz, *Swarm Intelligence: From Natural to Artificial Systems*, Oxford university press, 1999.
44 A. Adamatzky, B. D. L. Costello and T. Asai, *Reaction–diffusion Computers*, Elsevier, 2005.
45 N. R. Kheirabadi, A. Chiolerio, K. Szacilowski and A. Adamatzky, Neuromorphic liquids, colloids, and gels: A review, *ChemPhysChem*, 2023, **24**(1), e202200390.
46 P. L. Gentili, K. Szacilowski and A. Adamatzky, Approaching human intelligence through chemical systems: development of unconventional chemical artificial intelligence, *Front. Chem.*, 2023, (11), 1332647.
47 A. Adamatzky, Towards fungal computer, *Interface Focus*, 2018, **8**(6), 20180029.
48 M. R. Wasielewski, M. D. Forbes, N. L. Frank, K. Kowalski, G. D. Scholes, J. Yuen-Zhou, M. A. Baldo, D. E. Freedman, R. H. Goldsmith and T. Goodson III, *et al.*, Exploiting chemistry and molecular systems for quantum information science, *Nat. Rev. Chem.*, 2020, **4**(9), 490–504.
49 A. P. De Silva, *Molecular logic-based computation*, Royal Society of Chemistry, 2012.
50 M. Hagiya, A. Konagaya, S. Kobayashi, H. Saito and S. Murata, Molecular robots with sensors and intelligence, *Acc. Chem. Res.*, 2014, **47**(6), 1681–1690.
51 S. Murata, T. Toyota, S.-I. M. Nomura, T. Nakakuki and A. Kuzuya, Molecular cybernetics: challenges toward cellular chemical artificial intelligence, *Adv. Funct. Mater.*, 2022, **32**(37), 2201866.
52 C. Guindani, L. C. da Silva, S. Cao, T. Ivanov and K. Landfester, Synthetic cells: from simple bio-inspired modules to sophisticated integrated systems, *Angew. Chem.*, 2022, **134**(16), e202110855.
53 P. L. Gentili and J.-C. Micheau, Light and chemical oscillations: Review and perspectives, *J. Photochem. Photobiol., C*, 2020, **43**, 100321.
54 A. Zhabotinsky, Periodic processes of malonic acid oxidation in a liquid phase, *Biofizika*, 1964, **9**(306–311), 11.
55 R. J. Field and R. M. Noyes, Oscillations in chemical systems. iv. limit cycle behavior in a model of a real chemical reaction, *J. Chem. Phys.*, 1974, **60**(5), 1877–1884.
56 A. M. Turing, The chemical basis of morphogenesis, *Bull. Math. Biol.*, 1990, **52**, 153–197.
57 V. Castets, E. Dulos, J. Boissonade and P. De Kepper, Experimental evidence of a sustained standing turing-type nonequilibrium chemical pattern, *Phys. Rev. Lett.*, 1990, **64**(24), 2953.
58 T. S. Briggs and W. C. Rauscher, An oscillating iodine clock, *J. Chem. Educ.*, 1973, **50**(7), 496.
59 J. Gorecki and J. N. Gorecka, Information processing with chemical excitations–from instant machines to an artificial chemical brain, *Int. J. Unconv. Comput.*, 2006, **2**(4).
60 I. Nagypal and I. R. Epstein, Fluctuations and stirring rate effects in the chlorite-thiosulfate reaction, *J. Phys. Chem.*, 1986, **90**(23), 6285–6292.
61 I. Szalai and P. De Kepper, Pattern formation in the ferrocyanide-iodate-sulfite reaction: The control of space scale separation, *Chaos: Interdisciplinary J. Nonlinear Sci.*, 2008, **18**(2), 026105.
62 J. Horváth, I. Szalai and P. De Kepper, An experimental design method leading to chemical turing patterns, *Science*, 2009, **324**(5928), 772–775.
63 M. Orban and I. R. Epstein, A new type of oxyhalogen oscillator: the bromite-iodide reaction in a continuous flow reactor, *J. Am. Chem. Soc.*, 1992, **114**(4), 1252–1256.
64 I. Molnár and I. Szalai, Pattern formation in the bromate–sulfite–ferrocyanide reaction, *J. Phys. Chem. A*, 2015, **119**(39), 9954–9961.
65 P. Mougkogiannis and A. Adamatzky, Learning in ensembles of proteinoid microspheres, *R. Soc. Open Sci.*, 2023, **10**, 230936.
66 E. Itzhaki, Y. Elias, N. Moskovits, S. M. Stemmer and S. Margel, Proteinoid polymers and nanocapsules for cancer diagnostics, therapy and theranostics: In vitro and in vivo studies, *J. Funct. Biomater.*, 2023, **14**(4), 215.
67 S. R. Hameroff, *Ultimate Computing: Biomolecular Consciousness and Nanotechnology*, Elsevier, 2014.
68 P. Mougkogiannis and A. Adamatzky, Morphologies of proteinoids, 2023.
69 M. Caron, H. Touvron, I. Misra, H. Jégou, J. Mairal, P. Bojanowski and A. Joulin, Emerging properties in self-supervised vision transformers, Proc. IEEE/CVF international conference on computer vision, 2021, pp. 9650–9660.

70 X. Zheng, P. Zhang, Z. Fu, S. Meng, L. Dai and H. Yang, Applications of nanomaterials in tissue engineering, *RSC Adv.*, 2021, **11**(31), 19041–19058.
71 C. Ton-That, M. R. Phillips, M. Foley, S. J. Moody and A. P. Stampfl, Surface electronic properties of ZnO nanoparticles, *Appl. Phys. Lett.*, 2008, **92**(26), 261916.
72 S. Stewart, Q. Wei and Y. Sun, Surface chemistry of quantum-sized metal nanoparticles under light illumination, *Chem. Sci.*, 2021, **12**(4), 1227–1239.
73 Photochemical reaction – Photosensitization, Light Activation, Photoproducts, **https://www.britannica.com/science/photochemical-reaction**.
74 J. J. Lozeman, P. Führer, W. Olthuis and M. Odijk, Spectroelectrochemistry, the future of visualizing electrode processes by hyphenating electrochemistry with spectroscopic techniques, *Analyst*, 2020, **145**(7), 2482–2509.
75 Y. Ping, R. Sundararaman and W. A. Goddard III, Solvation effects on the band edge positions of photo-catalysts from first principles, *Phys. Chem. Chem. Phys.*, 2015, **17**(45), 30499–30509.
76 M. D. Hanwell, D. E. Curtis, D. C. Lonie, T. Vandermeersch, E. Zurek and G. R. Hutchison, Avogadro: an advanced semantic chemical editor, visualization, and analysis platform, *J. Cheminf.*, 2012, **4**(1), 1–17.
77 C. Sanchez, B. Julián, P. Belleville and M. Popall, Applications of hybrid organic–inorganic nanocomposites, *J. Mater. Chem.*, 2005, **15**(35–36), 3559–3592.
78 T. Park, N. Kim, D. Kim, S.-W. Kim, Y. Oh, J.-K. Yoo, J. You and M.-K. Um, An organic/inorganic nanocomposite of cellulose nanofibers and zno nanorods for highly sensitive, reliable, wireless, and wearable multifunctional sensor applications, *ACS Appl. Mater. Interfaces*, 2019, **11**(51), 48239–48248.
79 C. Sanchez, B. Lebeau, F. Chaput and J.-P. Boilot, Optical properties of functional hybrid organic–inorganic nanocomposites, *Adv. Mater.*, 2003, **15**(23), 1969–1994.
80 Aaryashree, S. Biswas, P. Sharma, V. Awasthi, B. S. Sengar, A. K. Das and S. Mukherjee, Photosensitive zno-graphene quantum dot hybrid nanocomposite for optoelectronic applications, *ChemistrySelect*, 2016, **1**(7), 1503–1509.
81 I. Rawal, R. K. Tripathi and O. Panwar, Easy synthesis of organic–inorganic hybrid nanomaterials: study of dc conduction mechanism for light dependent resistors, *RSC Adv.*, 2016, **6**(37), 31540–31550.
82 04 Principle and advantages of optical encoder | Tutorials | Rotation Angle Sensors | Products | Asahi Ka-sei Microdevices (AKM), **https://www.akm.com/content/www/akm/eu/en/products/rotation-angle-sensor/tutorial/optical-encoder.html**.
83 A. Ghasemi, N. Rabiee, S. Ahmadi, S. Hashemzadeh, F. Lolasi, M. Bozorgomid, A. Kalbasi, B. Nasseri, A. S. Dezfuli and A. R. Aref, *et al.*, Optical assays based on colloidal inorganic nanoparticles, *Analyst*, 2018, **143**(14), 3249–3283.
84 S. Hamedi, R. Negahdari and H. R. Ansari, Design plasmonic optical 4 × 2 encoder based on 2d photonic crystal ring resonator, *Plasmonics*, 2021, **16**, 1983–1990.
85 P. Nayak, A. Silberfarb, R. Chen, T. Muezzinoglu and J. Byrnes, Transformer based molecule encoding for property prediction, *arXiv*, 2020, preprint, arXiv:2011.03518-DOI: **10.48550/arXiv.2011.03518**.